Percolation study for the capillary ascent of a liquid through a granular soil

Manuel Antonio Cárdenas Barrantes

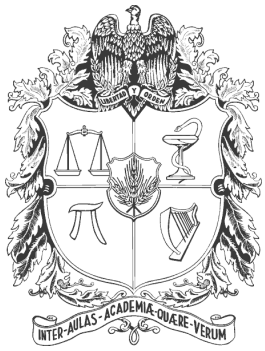

Universidad Nacional de Colombia
Facultad de Ciencias
Departamento de Física
Bogotá, D.C.
2016

Percolation study for the capillary ascent of a liquid through a granular soil

Manuel Antonio Cárdenas Barrantes

A dissertation submitted in partial satisfaction of the
requirements for the degree of
Master of Science (MSc) in Physics

Advisor
Dr. Rer. Nat José Daniel Muñoz

Research line
computational physics

Research group
Grupo de Simulación de Sistemas Físicos - SSF UN

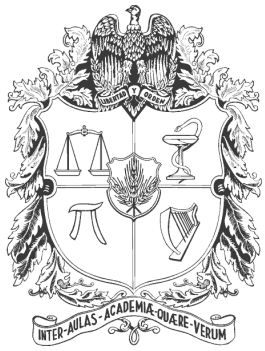

Universidad Nacional de Colombia
Facultad de Ciencias
Departamento de Física
Bogotá, D.C.
2016

Title in English

Percolation study for the capillary ascent of a liquid through a granular soil.

Título en español

Estudio de percolación del ascenso capilar de un liquido a través de un suelo granular.

Abstract: Capillary rise plays a crucial role in the construction of road embankments in flood zones, where hydrophobic compounds are added to the soil to suppress the rising of water and avoid possible damage of the pavement. Water rises through liquid bridges, trimers and enclosed volumes, and the void spaces among grains that could eventually take part of those capillary elements can eventually connect to form a path at disposal for capillary rise. The width and connectivity of that structure depends on the maximal half-length λ of a capillary bridge among the grains, which is a function of contact angle. Low λs generate a disconnect structure, with small clusters everywhere. On the contrary high λs create a percolating cluster of trimers and enclosed volumes that form a natural path for capillary rise. Hereby, we study the percolation transition of this geometric structure as a function of λ for a random dense packing of monodisperse spherical grains at volume fraction $\phi \simeq 0.63$. We determined a percolation threshold for $\lambda_c = (0.049 \pm 0.004)R$ (with R the radius of the spheres), less than one fourth of the mean distance between neighbouring grains at that volume fraction. In addition, all critical exponents for the transition are in good agreement with those of size percolation in three dimensions, suggesting that the formation of trimers (i.e. the main components of the connected path for capillary rise) can be considered as randomly independent, a possible consequence of the random positions for the grains. The study combines capillary structures and percolation theory to investigate capillary rise through a granular medium. It constitutes an interesting novel approach and a new step in the understanding of this rich phenomenon.

Resumen: El ascenso capilar desempeña un papel crucial en la construcción de terraplenes en carreteras construidas en zonas de inundación, donde se agregan compuestos hidrofóbicos al suelo para prevenir el aumento de agua y evitar posibles daños en el pavimento. El agua se sube a través de puentes de liquido, *trimers*, volúmenes encerrados de liquido, y los espacios vacíos entre los granos que eventualmente podrían tomar parte de esos elementos capilares. Estas estructuras pueden llegar a conectarse para formar un camino probable para el ascenso capilar. Los tamaños y conectividad de esa estructura depende de la longitud máxima media λ de los puentes capilares entre los granos, la cual es función del ángulo de contacto. Para λs pequeños se da lugar a una estructura disconexa, con pequeños *clusters* a lo largo de todo el sistema. Por el contrario, para λs grandes se crea un *cluster* percolante de *trimers* y volúmenes encerrados que forman un camino natural para el ascenso capilar. Estudiamos la transición percolante de esta estructura geométrica como función de λ para un *Random Dense Packing* de granos esféricos monodispersos, con una fracción de volumen $\phi \simeq 0.63$. Se determinó que el punto critico de percolación es $\lambda_c = 0.049 \pm 0.004)R$ (con R el radio de las esferas). Este valor es menos de una cuarta parte de la distancia media entre granos vecinos con esa fracción volumétrica. Además, también se calcularon los exponentes críticos que describen esta transición, los cuales están en buen acuerdo con los exponentes críticos para *site percolation*. Lo anterior sugiere que la formación de *trimers* (es decir, los componentes principales de los caminos para el ascenso

capilar) puede considerarse como aleatoria, consecuencia de las posiciones aleatorias de los granos. El estudio combina las estructuras capilares y la teoría de la percolación para investigar el ascenso capilar a través de un medio granular. Esto constituye un enfoque diferente y un nuevo paso en la comprensión de este fenómeno.

Advisor
Dr. Rer. Nat José Daniel Muñoz

Bogotá, D.C., Noviembre 25 de 2016

A mi familia.

Agradecimientos

Quiero agradecer al profesor José Daniel Muñoz por su excelente guía durante este interesante proyecto, quien no solo contribuyó a mi formación académica sino también personal. Además, al profesor Nuno Araujo por recibirme un tiempo en su grupo de investigación, brindando valiosos aportes a este proyecto con sus innumerables ideas.

A mi familia, en especial a mis padres y a mi hermana, por su cariño, apoyo incondicional, comprensión, e infinita paciencia a lo largo de todo este proceso.

A mis amigos y compañeros de estudio, por sus aportes y compañia en este tiempo.

Contents

List of Tables

List of Figures

Introduction

Imagine you are building a sand castle on the beach. The consistency of that castle depends entirely on the degree of moisture in the sand. It needs to be wet enough to maintain water-air interfaces among the grains, but without entirely filling the spaces among grains. That cohesive force, known as the capillary force, is also responsible for the rise of a liquid through a granular or porous medium. Now just consider a pile of sand with its base covered by water. If grains are close enough, water will rise through the interstices of the grains by action of such capillary forces. This capillary rise plays a major role in the transport of fluids across porous and granular media. It is highly studied in many industrial processes, such as agriculture, construction, extraction of hydrocarbons, geophysical imbibition processes, infiltration from surface water, flow transport and wet granulation in powder industries. The field has achieved an intense interdisciplinary study in recent years, trying to model it at the microscopic scale to find its possible behaviour at the macroscopic scale. This effort has been mainly motivated by its applicability in extraction and filtered processes of oil and gas. Specially in unsaturated soil structures, like embankments, the capillary rise of water is a real concern, because water can damage the integrity of the structure [5]. The broad spectrum of possible solutions include the use of hydrophobic materials [5] or even the addition of active mechanisms to compensate for the deformations produced by capillary forces [6].

The flow of water through a granular medium is strongly determined by the geometry of the interconnected structure of pores among the grains. First models [7] represented that structure by sites (pore bodies) of arbitrary shape and position interconnected by

bonds (pore throats), whose sizes and shapes could be obtained from experimental probes [8, 9]. Many properties, like relative permeability [10] or drainage and imbibition [11] can be estimated from this simplified model. Likewise, it has been found that some of the parameters that describe pore sizes and pore-connectivity are relating with quantities characterizing water retention [12]. But many methods to describe the transport of liquid through granular materials base on percolation, the theory that studies how pores set at random forms a contacted path for the liquid to flow across the material [13, 14, 15]. Indeed, the pore structure is so complex that to some extent it can be modelled as random. A nice example of the success of the percolation theory applied to granular soil is given by Larson and co-workers [16], they found that the distribution of globule of residual oil in reservoir rock is entirely described by the topological properties of the medium.

In regards to capillary rising, more recent works focus on representing the liquid structures among grains (bridges, menisci and pore bodies) as real as possible, based either on experiments (as in X-Ray microtomography [3]) or in computer simulations [17, 18]. This modeling is able to reproduce water saturation and drying with the water volume as control parameter and to compute forces and pressures [18]. Together with experiments, they have succeeded identifying trimers (that is, the junction of three liquid bridges and a meniscus) as the minimal building block to build a pathway for rising water [18, 3]. The structure itself must strongly change with the maximal length of a capillary bridge (a function of contact angle [19]), and some studies in two dimensions have been performed to find when a connected structure first appears as either the contact angle [20] or the liquid volume [21, 22] increases.

Consider a random configuration of grains. Once grain positions are fixed, the possibility of building a path for capillary rise must strongly depend on the maximal length of a capillary bridge. If it is too short, the places where capillary bridges and trimmers could eventually form show a disconnected structure, and water will never rise by capillarity. But, if it is large enough, they could join together to build a connected path across the sample. Even before injecting water, that path tell us that it would be possible for the water to rise. How this geometrical structure sets, a classical percolation problem, could give us valuable insights on the understanding of this phenomena. The present work investigates how the set of trimers and enclosing pore bodies at disposal for capillary rising changes from a fully disconnected structure to a connected pathway as the critical

length of the capillary bridges increases in three-dimensional dense packings of monodisperse spheres. The goal is to find both the critical half-length λ_c of a capillary bridges to obtained a connected structure and some of the critical exponents characterizing this phase transition.

This thesis is outlined as follows: Chapter 1 deals with the basic physics of capillary interfaces such as liquid bridges. Next, chapter 2 introduces percolation, plus finite size scaling as a very useful technique to characterize it [23, 24, 25]. Chapter 3 shows the analysis of the resulting liquid structures by using tools of percolation theory and a description of the model we use. The thesis finishes summarizing the main conclusions and discussions in chapter 4.

CHAPTER 1

Capillary theory

Capillarity is the study of the interface between a fluid and a solid or another fluid [2]. It is also the science that takes care of the shape and evolution of bubbles, drops and liquid films [26, 2]. It also studies how liquid rises through a structure, for example the coffee through a sugar cube and, therefore, it has many applications in the study of the water and oil flows through rocky soils [27, 28]. Indeed, the forces that keep cohesion among the grains of wetted sand in a sand castle are capillary forces. This makes its study a fundamental topic to describe how the stability of a soil changes with increasing water content, a key aspect for landslides prevention.

Capillarity can also be understood as the study of phenomena where surface tension takes part. Surface tension acts as if the interface itself were a stretched elastic membrane, that allows, for instance, water striders to skate on it. The form of surface in equilibrium usually minimizes the total energy of this interface (i.e. minimizes its area) and the pressure difference on both sides of the surface is determined by the surface curvature.

We will now describe the fundamental concepts of capillarity and some of the most relevant models for this work.

1.1 Surface tension and Laplace's equation

In a bulk material, each molecule establishes bonds with similar ones. Half of such bonds must be broken to create an interface between two media, replacing them by new bonds with the molecules of the other material. This process requires a certain amount of energy per unit of area, called *surface tension*, γ [26, 2]. Consider, for instance, an interface between water and air. Liquid molecules attract stronger to each other (due to cohesion) than to the molecules in the air (due to adhesion). The net effect is an entering force at the surface that causes the liquid to behave as if the surface itself were covered with a stretched elastic membrane, supporting a pressure difference between both sides of the interface.

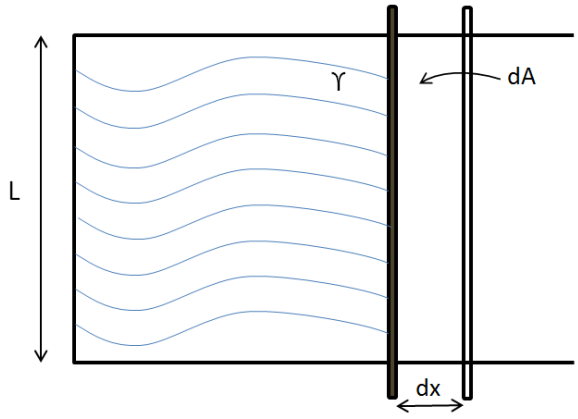

FIGURE 1.1. Soap film within a rectangular frame.

Surface tension can be understood either as an energy per unit area or as a force per unit length. This can be clearly seen if you consider a rigid metal frame of rectangular shape with a needle in the middle, touching both longest sides of the rectangle (Fig. 1.1). If you place a soap film within the rectangle at both sides of the needle, the needle itself will stay still; but if you break one of the two films, the other one will try to decrease its surface, pulling the needle all the way to the rectangle's end. Actually, there are two interfaces acting in this example, corresponding to the two surfaces of the film. As the needle moves by a distance dx, the work done by the film on the needle must equal the decrease on surface energy on both interfaces

$$2Fdx = 2\gamma Ldx \quad , \tag{1.1}$$

with F the force exerted by a single interface and L the needle length. Thus,

$$\gamma = \frac{F}{L} \tag{1.2}$$

can be understood as a force per unit length.

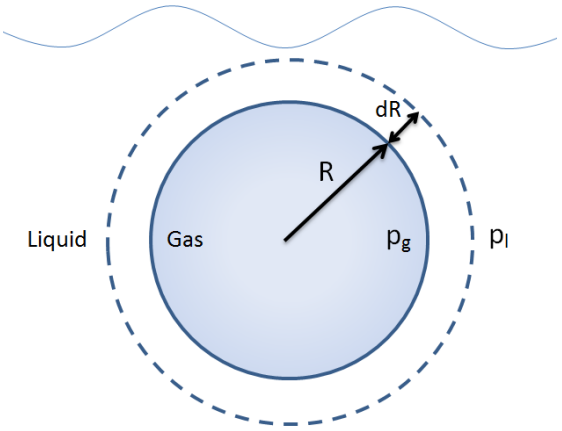

FIGURE 1.2. Gas bubble in water.

The pressure difference at both sides of the interface is determined by the surface curvature. Consider, for instance, a spherical bubble of a gas immersed in a liquid (Fig. 1.2). If the radius R of the bubble increases by a certain amount dR, the gas do a work $p_g dV$, with p_g the gas pressure and dV the volume increase. Similarly, the liquid do a work $-p_l dV$, with p_l the liquid pressure. At the same time, the bubble interface grows, and an energy γdA must be added to build the extra area dA. Because the network on the system should equal the energy increment,

$$p_g dV - p_l dV = \gamma dA \quad . \tag{1.3}$$

With $dV = 4\pi R^2 dR$ and $dA = 8\pi R dR$, Eq. (1.3) gives

$$\Delta p = p_g - p_l = \frac{2\gamma}{R} \quad . \tag{1.4}$$

This expression is a special case of a more general statement, known as the *Young-Laplace law*. Consider a curve AB on the surface and a point P on it. The curve divides the surface into two regions (Fig. 1.3). Across an element δl of AB, region 2 exerts a force $\gamma \delta l$ tangential to the surface, with γ the surface tension.

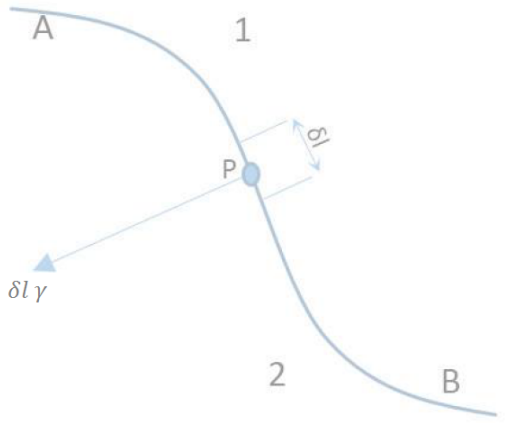

FIGURE 1.3. Surface tension definition at point P.

Now take a point P on the surface, and on the surface build a curve which distance from P along the surface equals to ρ. In that surface through that point take orthogonal lines AB and CD on the surface, with radii of curvature R_1 and R_2 respectively (Fig. 1.4). Taking into account the mechanical equilibrium, let us see the forces along the normal PN, f_n, at A, B, C and D. Since the surface tension pulls with a force $\gamma\delta l$, then the normal force at each point on the segment are $\gamma\delta l \sin(\phi)$ for the points A and B, and $\gamma\delta l \sin(\beta)$ for the other two points, given a total differential normal force equal to (for a small surface area, it means small ϕ and β):

$$\begin{aligned} df_n = &\quad 2\gamma\, dl\, \sin(\phi) + 2\gamma\, dl\, \sin(\beta) \\ = &\quad 2\gamma\, dl\, \rho \left(\tfrac{1}{R_1} + \tfrac{1}{R_2}\right) \quad . \end{aligned} \tag{1.5}$$

Integrating Eq. (1.5) around the whole circumference (one-quarter of a revolution, $0 < l < \rho$ and $0 < \theta_{Azimuth} < \frac{\pi}{2}$), and considering the pressure forces (due to the pressure P' and P''), we get:

$$\begin{aligned} (P'' - P')\pi\rho^2 = &\quad \pi\rho^2\gamma \left[\left(\tfrac{1}{R_1}\right) + \left(\tfrac{1}{R_2}\right)\right] \\ P'' - P' = &\quad \gamma \left[\left(\tfrac{1}{R_1}\right) + \left(\tfrac{1}{R_2}\right)\right] \\ \Delta P = &\quad \gamma \tfrac{1}{R_m} \quad , \end{aligned} \tag{1.6}$$

which is the Laplace's equation, where R_m is the mean radius of curvature.

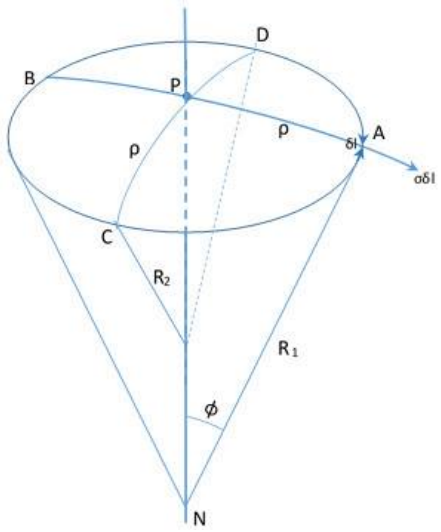

FIGURE 1.4. Diagram of capillary equilibrium [2].

In Eq. (1.6) we can see that because of the existence of surface tension, an arbitrary surface maintains mechanical equilibrium between two fluids at different pressures P'' and P'. In the absence of gravitational effects, the pressure P' and P'' are uniform throughout the respective phases, while the surface tension has the same value γ at all point in the surface. To include the effects of gravitational forces it is necessary to use the fact that P'' and P' vary with the height of the point considered [29, 26].

1.2 Three-phase systems, equilibrium at a line of contact and Young's equation

Capillary systems in granular media usually hold a solid phase and at least two fluid phases, for instance, there are surfaces subjected to surface tension that meet at a point P (Fig. 1.5). In the figure, an element of the line through P of length δl is subjected to the three forces $\gamma_1\delta l$, $\gamma_2\delta l$ and $\gamma_3\delta l$. When these forces are in equilibrium, we have

$$\gamma_1 + \gamma_2 + \gamma_3 = 0 \quad , \tag{1.7}$$

called the law of Neumann's triangle.

Continuing the analysis, take a liquid drop placed on a plain solid and smooth surface (Fig 1.6), from this we can define a contact angle θ ($0 \leq \theta \leq \pi$), as the angle subtended by the tangent to the liquid-gas boundary build at a point on the three-phase line of contact

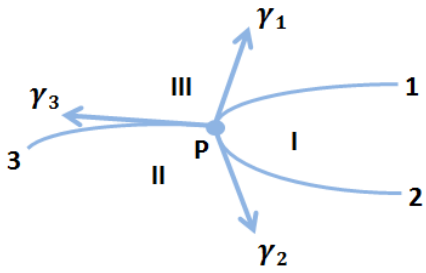

FIGURE 1.5. Equilibrium at contact point of three fluid phases [2].

and the tangent to the solid-liquid boundary build at the same point. Then we can write Eq. (1.7) as:

$$\gamma_{lg}\cos(\theta) = \gamma_{sg} - \gamma_{sl} \quad , \tag{1.8}$$

which is known as the Young's equation, where γ_{lg} is the surface tension of the liquid, γ_{sg}, the surface tension of the solid and γ_{sl}, the interfacial tension between the liquid and the solid [29, 30].

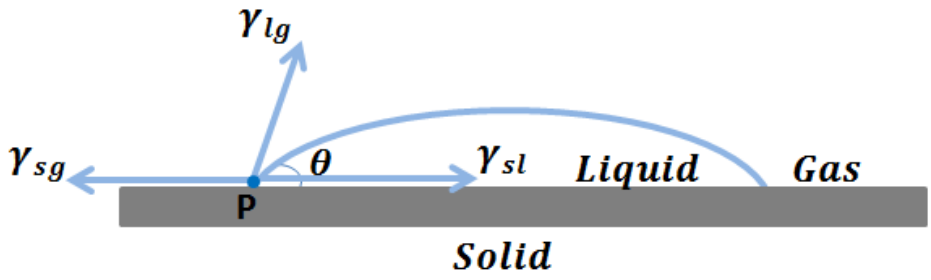

FIGURE 1.6. Equilibrium at a line of contact.

If the contact angle θ is in between 0 and $\pi/2$ we say that the liquid wets, here the adhesive force is higher than the cohesive force among the molecules of the liquid, but, if the contact angle θ is in between $\pi/2$ and π, the force due to the solid-gas superficial tension is lower than the force due to the solid-liquid superficial tension, it means that the cohesive force is higher than the adhesive force, and we said that the liquid does not wet the surface, those kind of materials are called hydrophobic materials.

1.3 Some examples of capillary phenomena

1.3.1 Capillary Tube, Jurin's law

Now that we have Young-Laplace's equation it is not difficult to make an approximation of the capillary rise phenomena in a tube (Fig. 1.7). Considering the two radii of curvature are equal to each other and to the radius of the capillary, R, from Young-Laplace equation we get

$$\begin{aligned} \Delta P = & \quad 2\frac{\gamma}{R} \\ = & \quad 2\frac{\gamma\cos(\theta)}{r} \quad , \end{aligned} \tag{1.9}$$

with θ the contact angle at the capillary wall and ΔP ($\Delta P = \Delta\rho\, g h$, where $\Delta\rho$ is the

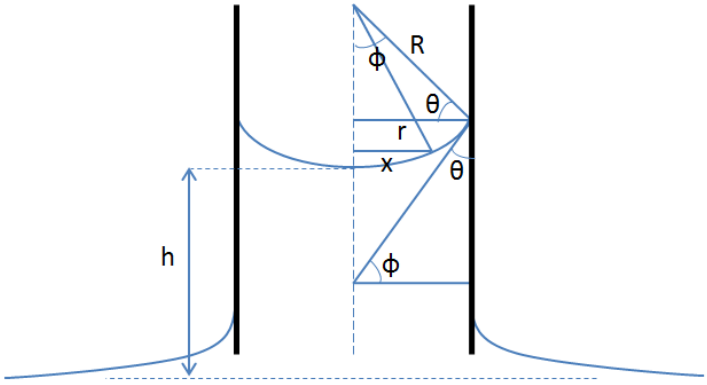

FIGURE 1.7. The meniscus in a capillary as a figure of revolution, with the radii of curvature $R_1 = R_2 = R$ [2].

difference in the density between the liquid and gas phases and g is the gravity field) is equal to the hydrostatic pressure drop in the column of liquid in capillary tube at the height of the meniscus above the flat liquid surface, h. It means that h is the height that the liquid can reach in tube due to the capillary interactions, known as the Jurin's law [2]. Then we can write Eq. (1.9) as

$$h = 2\frac{l^2}{r} \quad , \tag{1.10}$$

with $l^2 = \frac{\gamma\cos(\theta)}{\Delta\rho\, g}$, l is known as the capillary length, beyond which gravity becomes important and is generally of the order of few millimeters [2].

As was mentioned at beginning of the section, the previous lines are just a good approximation of the problem, the real treatment must take into account the deviation of the meniscus from sphericity ($\Delta P = \Delta\rho\, gy$ at each point on the meniscus), also from the real geometry of the problem the radii of curvature, R_1 and R_2, are not the same.

1.3.2 Drop deposited on a fiber

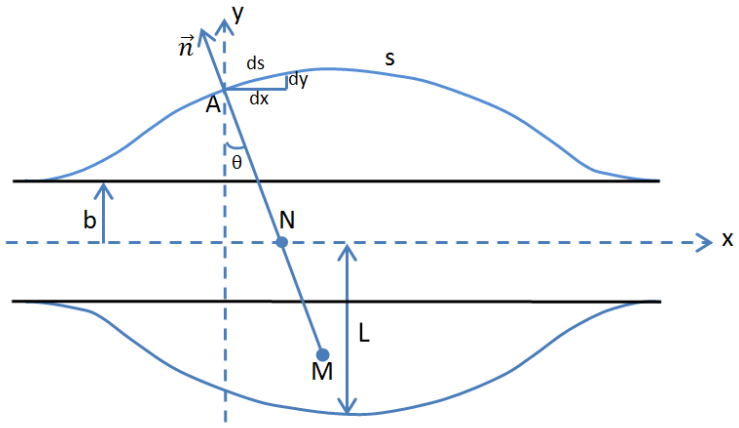

FIGURE 1.8. Drop deposited on a fiber [2].

Think of a drop of radius R deposited on a fiber of radius b ($b << L$) (Fig. 1.8), where its profile $y(x)$ is given from the Young-Laplace's equation, Eq. (1.6), and a geometrical analysis. Taking θ as the angle between the normal vector to the profile of the drop, $\vec{n}$, and the vertical direction, and s the curvilinear coordinate along the profile [2], we easily see that:

$$ds = -R_1 d\theta \tag{1.11}$$

$$y = R_2 \cos(\theta) \quad . \tag{1.12}$$

Then Eq. (1.6) for this case take the form

$$-\frac{d\theta}{ds} + \frac{\cos(\theta)}{2} = \frac{\Delta p}{\gamma} = cst \quad . \tag{1.13}$$

Because we have that $dy = ds\,\sin(\theta)$ and $dx = ds\,\cos(\theta)$, we can write ds as $ds = dx(1+\dot{y}^2)^{\frac{1}{2}}$, ($\dot{y} = \frac{dy}{dx}$), also $\frac{d\theta}{ds} = \frac{d\theta}{dx}\left((1+\dot{y}^2)^{-\frac{1}{2}}\right)$ and $\ddot{y} = \left(1+\tan^2(\theta)\right)\frac{d\theta}{dx}$. Then finally we get

$$-\frac{\ddot{y}}{(1+\dot{y}^2)^{\frac{3}{2}}} + \frac{1}{y\,(1+\dot{y}^2)^{\frac{1}{2}}} = \frac{\Delta p}{\gamma} \quad . \tag{1.14}$$

To solve Eq. (1.14) you can multiply it by $y\dot{y}$ and becomes a derivative of a product, and integrating

$$\frac{d}{dx}\left[\frac{y}{(1+\dot{y}^2)^{\frac{1}{2}}}\right] = \frac{\Delta p}{2\gamma}\frac{d\left[z^2\right]}{dx}$$
$$\frac{y}{(1+\dot{y}^2)^{\frac{1}{2}}} = \frac{\Delta p}{2\gamma}y^2 + C \quad . \tag{1.15}$$

If we see the boundary conditions at $y = b$ we get that $\dot{y} = 0$, from which it follows that $C = b - \frac{\Delta p}{2\gamma}b^2$, then

$$\frac{y}{(1+\dot{y}^2)^{\frac{1}{2}}} = \frac{\Delta p}{2\gamma}\left(y^2 - b^2\right) + b \quad . \tag{1.16}$$

If we check Eq. (1.16) at $y = L$ with $\dot{y} = 0$ we can approximate the overpressure Δp, for a very large drop, $(L >> b)$, to

$$\Delta p = \frac{2\gamma}{L+b} \quad . \tag{1.17}$$

1.3.3 Meniscus on a Fiber

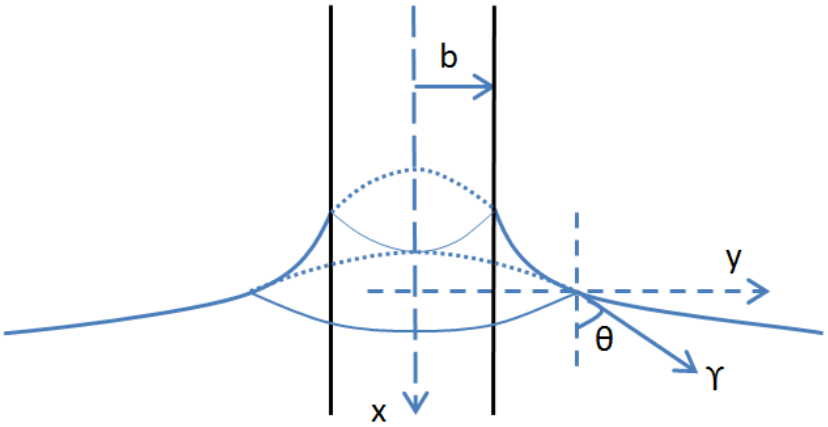

FIGURE 1.9. Rising water on a fiber [2].

Now we are going to study the rise of a liquid on a wetted fiber and its profile $(y(x))$ (Fig. 1.9). Neglecting the influence of gravity and taking $L \to \infty$, which gives $\Delta p = 0$

(the liquid in the meniscus is in equilibrium with the liquid bath) in Eq. (1.17) we get

$$\frac{y}{(1+\dot{y}^2)^{\frac{1}{2}}} = b \quad , \tag{1.18}$$

it can be solve with a change of variable, $\frac{y}{b} = \cosh(u)$, so $dx = b\,du$ and integrating

$$\begin{aligned} bu &= x + C \\ \cosh\left(\frac{x+C}{b}\right) &= \cosh(u) \\ y = b\cosh\left(\frac{x+C}{b}\right) &\quad , \end{aligned} \tag{1.19}$$

taking into consideration the boundary conditions (at $x = 0$ we have $y = b$, then $C = 0$):

$$y = b\,\cosh\left(\frac{x}{b}\right) \quad . \tag{1.20}$$

1.3.4 Catenoidal soap film suspended between two coaxial circular rings

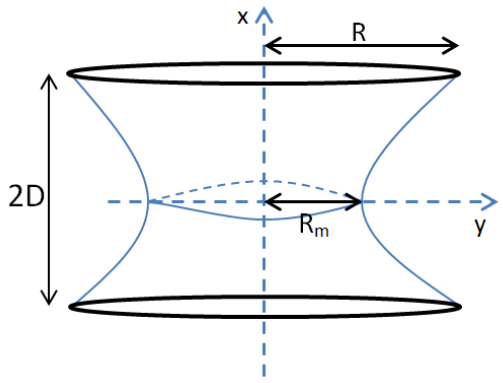

FIGURE 1.10. Catenoidal soap film [2].

Consider a soap film between two coaxial circular rings of the same radius R and distance $2D$ between them (Fig. 1.10). We have that the difference of pressure in the film is equals to zero ($\Delta p = 0$) because the pressure is the same in both sides of the film; for the same reason the curvature of the film is zero. Taking into account the previous lines we get that the profile of the film, $y(x)$, follows a catenary curve connecting both rings Eq. (1.20), with $b = R_m$ the radius of the circle described at $x = 0$

$$\frac{y}{R_m} = \cosh\left(\frac{x}{R_m}\right) \quad . \tag{1.21}$$

Applying the boundary conditions at $x = D$ we have

$$\frac{R}{R_m} = \cosh\left(\frac{D}{R_m}\right) \quad , \tag{1.22}$$

it has two solutions that become identical at $R \approx 1.509D$; it means that for distances D greater than maximum value $R/1.509$ the film will break.

1.3.5 Capillary liquid bridge

Let us now consider a liquid bridge between two equal sized spheres of radius R (Fig. 1.11). Neglecting the gravitational effects, we can write the pressure across the air-liquid interface of the liquid in a dimensionless form, from Eq. (1.6) as following [31]:

$$2H = \frac{y''}{(1+y'^2)^{\frac{3}{2}}} - \frac{1}{y(1+y'^2)^{\frac{1}{2}}} \quad , \tag{1.23}$$

where $X = \frac{x}{R}$ and $Y = \frac{y}{R}$ are the dimensionless coordinates, and H is the mean curvature,

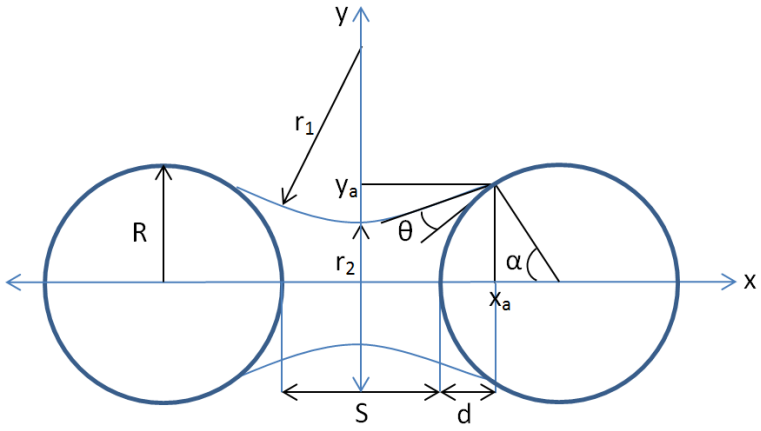

FIGURE 1.11. Liquid bridge between two equal spheres [31].

$H = \frac{\Delta\rho\, R}{2\gamma_{lg}}$. Here $Y(X)$ shows the meridian profile of the liquid bridge. Let us obtain the expressions for Y_i', Y_i'' and the initial condition $Y_a = \frac{y_a}{R}$ from the boundary conditions at $X = X_a$ ($Y = \sin(\alpha)$ and $Y' = \cot(\alpha + \theta)$, α the half-filling angle). Substituting

$K = Y'^2 + 1$ in Eq. (1.23) we get a Bernoulli equation which can be integrated:

$$\begin{aligned} \frac{dK}{dY} - \frac{2K}{Y} &= 4H\,K^{\frac{3}{2}} \\ \frac{Y}{(1+Y'^2)^{\frac{1}{2}}} + H\,Y^2 &= \sin(\alpha)\,\sin(\alpha+\theta) + H\,\sin^2(\alpha) = C \quad . \end{aligned} \tag{1.24}$$

Because the liquid bridge is symmetrical we have that $Y'(0) = 0$, then

$$Y_a = \begin{cases} C & \text{if } H = 0 \\ \frac{-1+(1+4H\,C)^{\frac{1}{2}}}{2H} & \text{if } H \neq 0 \end{cases} \quad , \tag{1.25}$$

and

$$Y'_i = \sqrt{\left(\frac{Y_i}{C - HY_i^2}\right)^2 - 1} \quad , \tag{1.26}$$

$$Y''_i = \frac{1 + Y_i'^2}{Y_i} + 2H(1 + Y_i'^2)^{\frac{3}{2}} \quad . \tag{1.27}$$

There are many methods to solve Eq. (1.26) and Eq. (1.27), in particular iterative ones, for example the method of Bashforth and Adams [32], the Rayleigh Method [33] and Lane Method [34], which nowadays are not too difficult to implement thanks to the high speed computers. Particularly, let us see the approximation propose by Fisher [35], called the toroidal approximation, this because it is and excellent approximation compared to experimental data [31, 36, 37].

1.3.5.1 Toroidal approximation of a static liquid bridge

We consider a liquid bridge between two equal sized spherical grains of radius R (Fig. 1.11). Thinking of a very small spherical grains, the gravitational effects can be neglectted, so the liquid bridge has a constant pressure [31] with the same mean curvature [17]. We just consider the upper right quadrant in (Fig. 1.11), where the liquid and solid profiles are considered as an arc of circumferences and are described by [19, 38, 36]:

$$y_L(x) = (r_1 + r_2) - (r_1^2 - x^2)^{1/2} \quad and \tag{1.28}$$

$$y_S(x) = \left(R^2 - (x - \frac{S}{2} - R)\right)^{1/2} \tag{1.29}$$

respectively. With $r_1 = y_a + r_2(1-\sin(\alpha+\theta))$ and $r_2 = \frac{1+\frac{S}{2}-\cos(\theta)}{\cos(\alpha+\theta)}$ (related with the bridge's thickness), the principal radii of curvature, which are described as function of α, the half-filling angle, and θ the contact angle, or by $x_a = \frac{S}{2} + R - R\cos(\alpha)$ and $y_a = R\sin(\alpha)$, the coordinate of the point of contact between the liquid and the spherical grain. Besides, S is the distance between surfaces of the spherical grains and $d = R - R\cos(\alpha)$, the wetted part of the grains.

The volume of the bridge is then define by the integral:

$$\frac{V}{2\pi} = \int_0^{x_a} y_L^2(x)dx - \int_{\frac{S}{2}}^{x_a} y_S^2(x)dx \tag{1.30}$$

with the following solution:

$$\begin{aligned}\frac{V}{2\pi} = \left[(r_1+r_2)^2 + r_1\right] x_a - \frac{x_a^3}{3} - (r_1+r_2)\left[x_a(r_1^2 - x_a^2)^{\frac{1}{2}} + r_1^2\ \arcsin(x_a/r_1)\right] \\ -\frac{1}{3}\left(x_a - \frac{S}{2}\right)^2\left[3R - x_a + \frac{S}{2}\right] \quad .\end{aligned} \tag{1.31}$$

The maximum amount of liquid that the bridge can hold, V_{max}, is reached when $r_1 \to \infty$ with the limit half-filling angle $\alpha_m = \frac{\pi}{2} - \theta$:

$$V_{max} = 2\pi\left[x_a y_a^2 - \tfrac{1}{3}d^2(3R-d)\right] \tag{1.32}$$

$$= \tfrac{2}{3}\pi R^3\left[3\cos^2(\theta)\left(\tfrac{S}{2R} + 1 - \sin(\theta)\right) - (1-\sin(\theta))^2(2+\sin(\theta)\right] \quad . \tag{1.33}$$

Also, there exist a critical distance where the bridge will break, S_c. This distance was first theorical studied by Lian et. al. [39] with a good experimental fiting [40, 41]. They found that

$$\frac{S_c}{R} = \left(1 + \frac{\theta}{2}\right)\left(\frac{4\pi}{3}V\right)^{\frac{1}{3}} \quad . \tag{1.34}$$

If we replace V_{max} from Eq. (1.32) in Eq. (1.34), we can get a good approximation of the maximum distance S_c at which the bridge is stable as a function of the contact angle θ,

$$\frac{S_c}{R} = \frac{(2+\theta)\pi^{\frac{1}{3}}\left(4\sin(\theta) - 4\sin(\theta)\cos^2(\theta) + 3\frac{S_c}{R}\cos^2(\theta) + 6\cos^2(\theta) - 4\right)^{\frac{1}{3}}}{2(3)^{\frac{1}{3}}} \tag{1.35}$$

the two spherical grains have to be located at a distance $S \leq S_c$ for a fixed values of the contact angle, otherwise, the bridge will break apart (Fig. 1.12), deduced from data in [19]. These results should be taken with some care, because the maximal distance for a capillary bridge obtained here can be much larger than the one of $0.655R$ obtained when the pressure difference across the capillary surface can be neglected (Sec. 1.3.4). Nevertheless, such a discrepancy is not relevant for our work; we only need to know that such a maximal distance exists as a function of the grains' radius and contact angle.

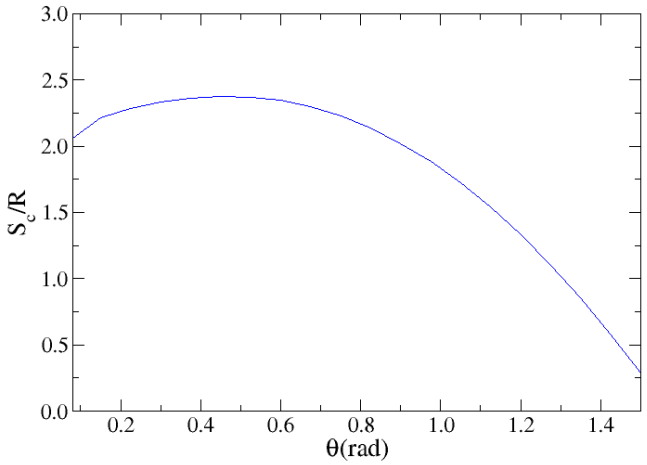

FIGURE 1.12. Maximal separation distance S_c for a capillary bridge as function of the contact angle θ in the toroidal approximation.

1.4 Capillary rising liquid in a monodisperse random packing

From a microscopic point of view, water can rise if the grains are close enough to build capillary bridges among them, appearing when solid particles are joined together by small amounts of liquid, but not enough to fully cover the solid surfaces. We can see this kind of structures in flotation systems, moist solids or wet granular materials, as in sand castles. The shape of a capillary bridge between two identical spherical grains is not strongly affected by gravity. It essentially depends on the contact angle θ, the liquid-gas surface tension γ, the liquid volume V and the distance S between the grains [31].

There is a maximal distance among grains S_c a capillary bridge can overcome, which we are going to call 2λ on this work. If $S < 2\lambda$, a capillary bridge may eventually be established for some V; otherwise, there is no possible path between the grains for the water to rise. This limit can be estimated through some theoretical approximation, like the toroidal approximation method [35], explained before, or by numerical simulations.

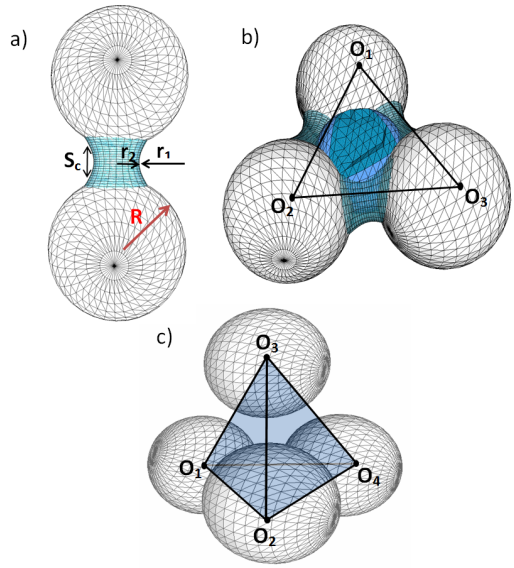

FIGURE 1.13. Main capillary structures. (a) Liquid bridge with separation distance S. (b) Trimer, built by three liquid bridges (light blue) and a meniscus (dark blue). (c) A liquid volume enclosed by four trimers.

In a dense monodisperse packings, spheres have in average approximately eight contacts that can hold a liquid bridge for each grain. It means that there is a high probability that two or more bridges connect to form larger liquid structures (liquid clusters) and, eventually, build a path for the rising water. Liquid clusters are made up of three basic units: liquid bridges, trimers and entirely filled pore bodies (Fig. 1.13). From a theoretical point of view, it would be possible to join two bridges with a meniscus but, according to micro-tomographies on experimental random granular arrays of monodisperse spheres [3] that kind of structures do not exist. Instead, if three grains are so close that liquid bridges are formed between every two of them and the three bridges touch each other, the region in the center (a meniscus) is filled with liquid. The resulting structure is what we call a *trimer* [18].

The minimal connected structures in partially filled monodisperese random granular packings are trimers, the junction of three liquid bridges and a meniscus [18] (Fig. 1.14). A trimer will eventually form for some water content if three grains are so close together

that the distances between any two of them are shorter than S_c Eq. (1.35) and the angles between every two bridges are smaller than $\pi - 2\theta$, which comes straightforward from the toroidal approximation. Two trimers are assumed connected if they share a bridge, and connected trimers can eventually enclose filling volumes (Fig. 1.14). Trimers and enclosed volumes form the structure for capillary rising. If S_c is small, the structure is a disconnected set of clusters, because there is less probability to build bridges between two grains. On the contrary, if S_c is large enough, there is a connected path across the sample, i.e. a percolating passage for the liquid to rise.

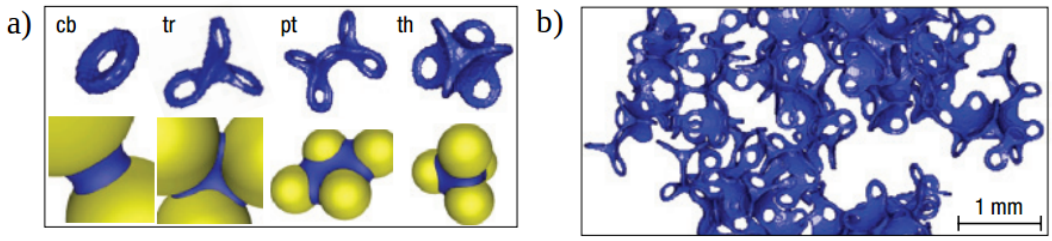

FIGURE 1.14. Liquid morphologies in a wet granular pile of with glass beads with average diameter of $280\mu m$. (a) Capillary bridge (cb), trimer (tr), pentamer (pt) and filled tetrahedra (th) as obtained from X-ray tomography. (b) Fraction of a large percolating liquid cluster. Figure taken from [3].

Early works on this percolating structure just considered the geometry of the space among grains as a set of volumes (sites) connected by throats (bonds) [42, 12]. Recent works, in contrast, intend to represent both the pore space and the liquid structures as close as possible to their real shape, constructed based on the exact geometrical positions of a previously simulated granular packings [43, 18]. For instance, Melnikov and co-workers [18], using volume as a control variable, propose a model for fluid saturation in random packings that can describe arbitrary liquid contents from dry to full saturation. This way, a pore network is extracted directly from the topology of the sphere packing. Pore bodies can be empty, partially filled with liquid separated by menisci or entirely filled by liquid. They found that, as water volume increases, the pressure difference across the capillary surface decreases as the same rate as the surface fraction covered by water increases. Consequently, cohesion forces among grains remain approximately constant, in good agreement with experimental measurements [3]. This work show that the detailed study of the shape of the capillary structures is an excellent method to calculate the mechanical properties of the system. Nevertheless, reproducing the exact geometry of the entire liquid structure and the void pores asks for high computational power. In principle,

all differential equations describing each one of basic structures present in the system must be solved, such as liquid bridges for all pairs of close grains and trimers for all trios of first neighboring spheres. Instead, we will follow an approximate scheme, but maintaining trimers as the basic structure for capillary rising, as will be described in Chapter 3.

CHAPTER 2

Percolation theory

The study of porous media is not an easy task, because of the deep complexity of its structure. The internal geometry of these materials is highly disorganized, to the point of being considered totally random [44]. For this reason it is impossible to describe porous media using cell parameters or symmetries. Instead, stochastic theories have been successful to describe some properties of these materials, and one of the most used is percolation theory [12].

2.1 What is percolation?

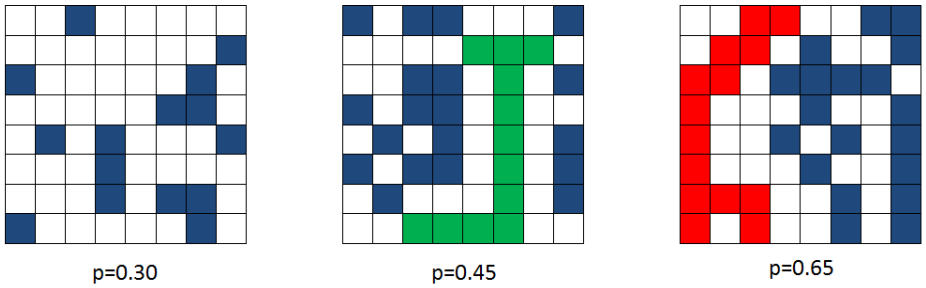

FIGURE 2.1. Example of the site percolation problem in a square lattice for different values of the occupation probability, p. Blue (white) cells represent occupied (non-occupied) sites. Green and red sites are examples of clusters, and the red one is a percolating cluster).

Let us explain what percolation is with an example. Imagine a large square lattice composed of $L \times L$ sites, with L so large that boundary effects can be neglected. Each square, or *site*, is occupied with probability p, independently of the other sites. A set of occupied first neighboring squares is called cluster; that is, two occupied sites sharing a side belong to the same cluster. If p is small, all clusters are small and disconnected. But, if p is large, there is a cluster, called the *percolating cluster*, passing through the entire system, from one side to the opposite one (Fig. 2.1), and we say that the system *percolates*. In an infinite system, there exists a critical occupation probability, p_c, such that there is no percolating cluster for $p < p_c$, while for $p > p_c$ the system percolates. We call p_c the *percolation threshold*. The percolation probability Π_∞, that is the probability for an infinite system to percolate, is, thus, a step function. For finite systems, the so called *effective percolation probability* Π^{eff} is a sigmoid, whose width decrease by increasing system size L (Fig. 2.2). Percolation theory deals with the number and properties of these clusters around that critical point for many kind of networks, like configurations of spheres, bones or pores, among many others. The example explained above is called site percolation [23]. Actually, we will use a variant of the site percolation problem in the present work.

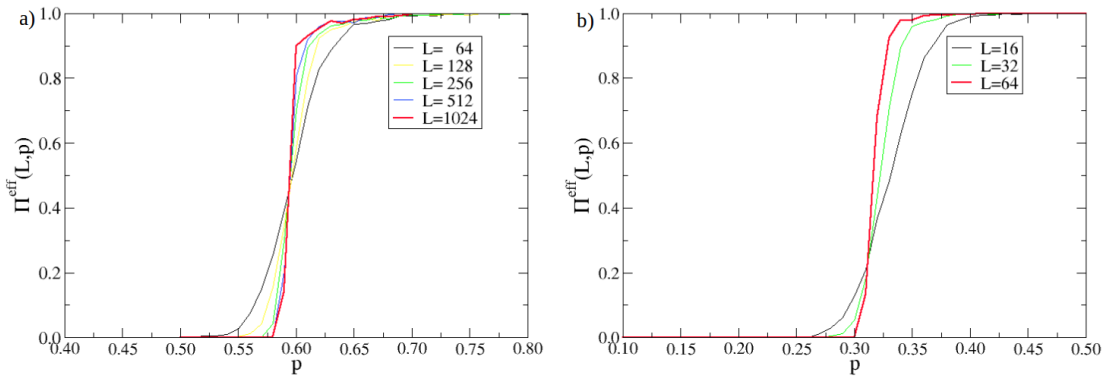

FIGURE 2.2. Effective percolation probability Π^{eff} as a function of the occupation probability p for site percolation for several system sizes, using the DPL algorithm (see Section 3.3). (a) Two-dimensional systems. (b) Three-dimensional systems.

Percolation is a purely geometrical problem and is the simplest model that undergoes a phase transition showing a drastic change in the spatial structure of the system [1]. It is highly relevant to describe with a good quality many physical phenomena, like oil recovery from porous media [45], connectivity in networks [46], fracture patterns and water flow [44], among many others [23, 47, 48].

2.2 Critical exponents for site percolation

Besides the percolation's threshold, the topological properties of the clusters are characterized by several quantities, such as the cluster size frequency, $N(s,p;L)$, the cluster number density, $n(s,p)$, the cluster size, $S_\xi(p)$, the mean cluster size, $\chi(p)$, the correlation length, $\xi(p)$ and the probability that a site belongs to the percolating cluster, $P_\infty(p)$, with L the size of the system and s the cluster size. Near to the percolation threshold all these quantities obey scaling laws that are independent from the microscopic details and only depend on the dimensionality and connectivity of the system [44].

Because the exponents describing the behavior of the quantities named before are of the form

$$X \propto |p - p_c|^b \quad , \tag{2.1}$$

with b the critical exponent, it is necessary to know first a very precise value for the percolation threshold p_c in order to get accurate exponent values. A biased value for p_c can lead an error in the estimation of the critical exponents. To solve this issue, Levinshtein et al. introduced and effective method to determine both the critical exponents and the critical threshold of an infinite system from data of finite systems of several finite sizes L [49, 23]. This procedure, known as *finite size scaling*, is the one we will use in our study.

2.2.1 Correlation length

The correlation function $g(r)$ is the probability that an occupied site and another site at a distance r from the first one belongs to the same cluster, but not to the percolating cluster. In general, this function usually decays as an exponential,

$$g(r) = \exp\left(-\frac{r}{\xi}\right) \quad , \tag{2.2}$$

where ξ, called the *correlation length*, is proportional to the average cluster diameter.

The characteristic cluster size s_ξ is proportional to the correlation length [23], as follows:

$$s_\xi \propto \xi^D \quad . \tag{2.3}$$

Here D is known as the fractal dimension of the percolating cluster. As the characteristic cluster size diverges for $p \to p_c$, from Eq. (2.3) the correlation length diverges as well (Fig. 2.3). This divergence is described by the critical exponent ν,

$$\xi(p) \propto \mid p - p_c \mid^{-\nu}, \quad p \to p_c \quad . \tag{2.4}$$

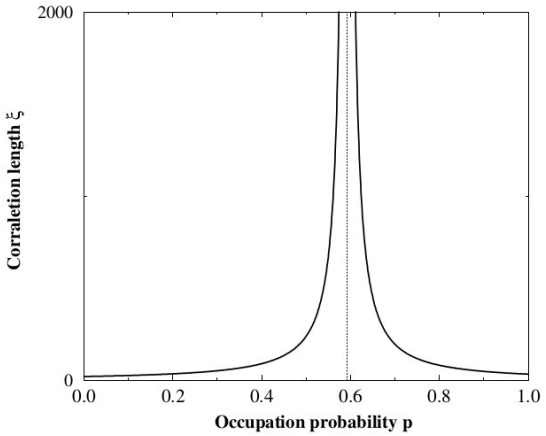

FIGURE 2.3. Correlation length vs. the occupation probability [4].

In practice, ν is more often estimated by considering the finite-size scaling of one or more of the properties of the system [23]. First, the effective percolation probability $\Pi^{\text{eff}}(L,p)$ as a function of p (Fig. 2.2) is fitted by an error function $\text{erf}(p)$ [23],

$$\Pi^{\text{eff}}(L,p)(p) \simeq \frac{1}{2}\,\text{erf}\left[\frac{p - p_c^{\text{eff}}(L)}{\Delta(L)}\right] + \frac{1}{2} \quad \text{, with} \quad \text{erf}(x) = \frac{1}{2\pi}\int_{-\infty}^{x} e^{-\frac{t^2}{2}}\,dt \quad . \tag{2.5}$$

Here, $p_c^{\text{eff}}(L)$ is called the effective percolation threshold for a system of size L, and $\Delta(L)$ is the effective width of this sigmoidal.

For determining the exponent ν, they take advantage of the scaling law for the effective width $\Delta(L)$, given by

$$\Delta \propto L^{-\frac{1}{\nu}} \quad . \tag{2.6}$$

Also, it is possible to find a good estimation for the percolation threshold, p_c, plotting $p_c^{\text{eff}}(L)$ against $L^{-\frac{1}{\nu}}$, which should draw a straight line intercepting the y-axis at p_c (Fig. 2.5). This is the standard procedure to estimate ν and p_c.

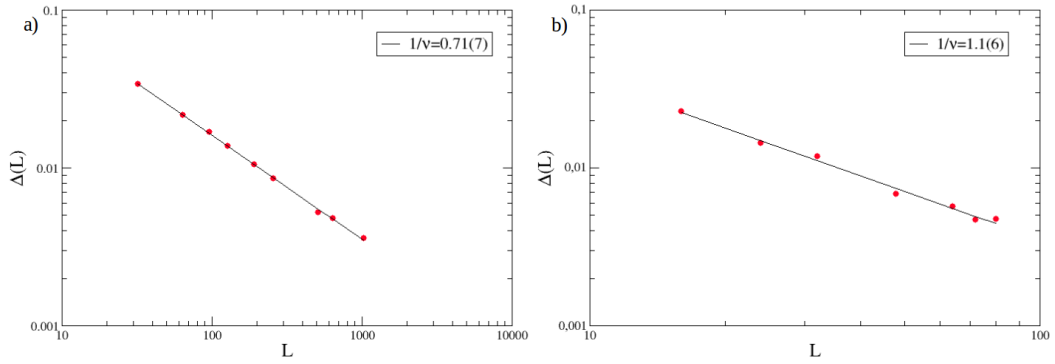

FIGURE 2.4. Width $\Delta(L)$ of the effective percolation probability $\Pi^{\text{eff}}(L,p)$ for site percolation (Fig. 2.2) vs. system size L in (a) two dimensional and (b) three dimensions. The slope gives $\nu = 1.40(5)$ and $\nu = 0.90(6)$ for two and three dimensions, respectively. Using the DPL algorithm (see Section 3.3).

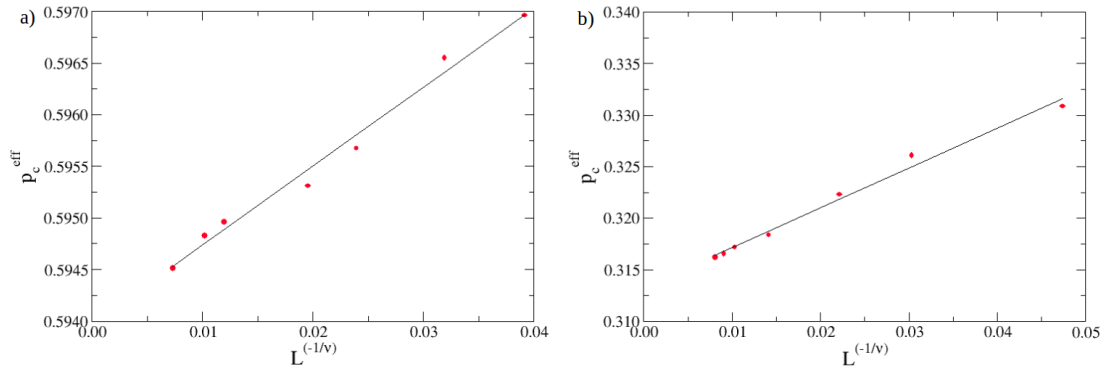

FIGURE 2.5. Effective percolation threshold $p_c^{\text{eff}}(L)$ against $L^{-\frac{1}{\nu}}$ for site percolation. The linear fit (continuous line) estimates a cut with the vertical axis at: (a) $p_c = 0.593(5)$ for two-dimensional systems and (b) $p_c = 0.313(3)$ for three-dimensional ones. Using the DPL algorithm (see Section 3.3).

2.2.2 Order parameter

The control parameter of the percolation transition is the probability p. The order parameter $P_\infty(p)$ is the probability that a site belongs to the percolating cluster. When $p < p_c$, there is no percolating cluster, so $P_\infty(p) = 0$. Close above the critical threshold, $P_\infty(p)$ grows as a power law with critical exponent β,

$$P_\infty(p) \propto (p - p_c)^\beta, \quad p \to p_c^+ \quad . \tag{2.7}$$

It is difficult to determine the critical exponents for the order parameter directly. Instead, finite-size scaling techniques are employed. Let us remember that the correlation length

grows like $\xi \propto |p-p_c|^{-\nu}$ Eq. (2.4). Thus $|p-p_c| \propto \xi^{\nu}$ and $P_\infty(p) \propto \xi \propto \xi^{\frac{\beta}{\nu}}$. If the system is finite of size L and $\xi > L$, clusters cannot be larger than L. Thus, L takes the place of ξ as the characteristic length, and

$$P_\infty(p_c, L) \propto L^{-\frac{\beta}{\nu}} \quad . \tag{2.8}$$

Fig. 2.6 shows how this relation can be used to estimate β.

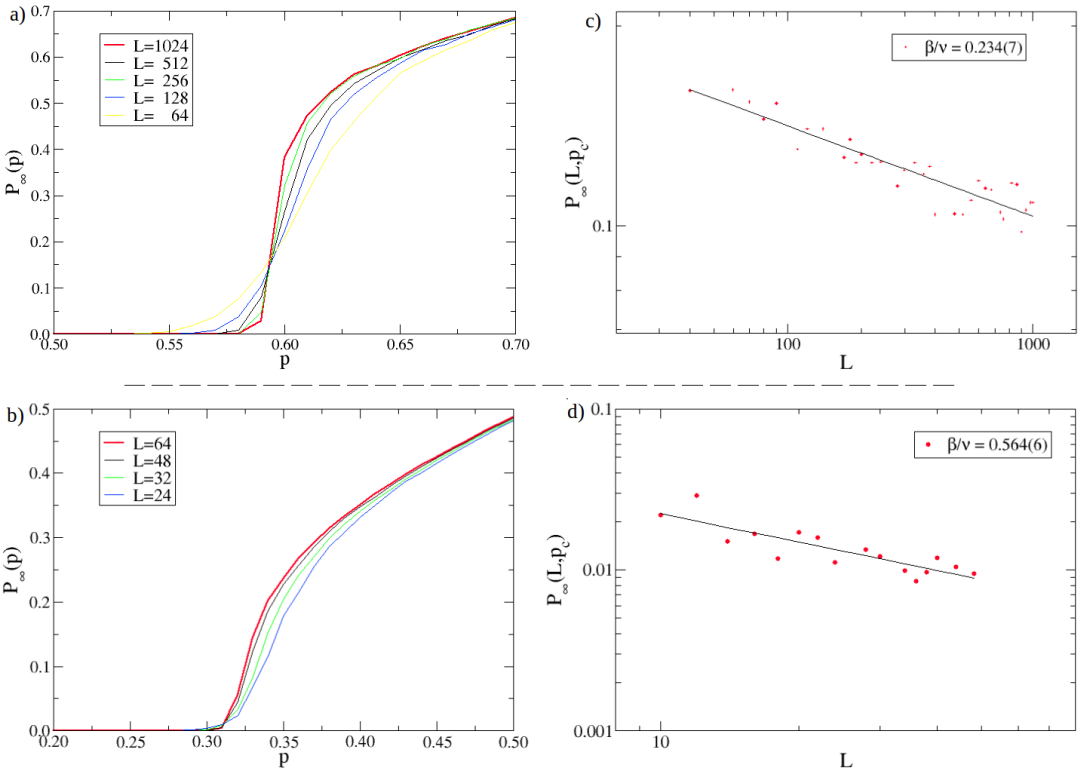

FIGURE 2.6. (left) Numerical results for the order parameter $P_\infty(p)$ for site percolation on (a) 2D and (b) 3D square lattices of several system sizes L, using the DPL algorithm (see Section 3.3). (right) Effective value of the order parameter at p_c against L for (c) two and (d) three dimensional systems. The slopes give $\beta = 0.16(4)$ and $\beta = 0.48(5)$ for two and three dimensions, respectively.

2.2.3 Cluster number density

Consider a cluster of size s (a s-cluster) of a certain shape, with t unoccupied nearest neighbors (the perimeter). The probability that such a cluster appears in the set of $s+t$ sites is $p^s(1-p)^t$. The probability that a random site belongs to that cluster is $sp^s(1-p)^t$. If the whole system is of size L, such a situation can take place approximately L^d/s times, with d the dimension of the system. Thus, the probability that a random site belongs to

a cluster of size s and that fixed shape is $L^d p^s (1-p)^t$. Next, let us consider that there are $g(s,t)$ different cluster shapes of size s and perimeter t. So, let us define the total number of clusters of size s in a system of size L with occupation probability p as [1]

$$N(s,p;L) = L \sum_{t=1}^{\infty} g(s,t)(1-p)^t p^s \quad . \tag{2.9}$$

The cluster number density, a more useful quantity, is defined as

$$n(s,p) = \frac{N(s,p;L)}{L} = \sum_{t=1}^{\infty} g(s,t)(1-p)^t p^s \quad . \tag{2.10}$$

For clusters sizes $s << s_\xi$ (s_ξ, the characteristic cluster size, which is the typical size of the largest cluster), the cluster number density decays approximately as a power law in s ($n(s,p) \propto s^{-\tau}$), and faster for $s >> s_\xi$, that is

$$n(s,p) \propto s^{-\tau} exp\left(\frac{-s}{s_\xi}\right), \quad \text{for } p \to p_c, s << s_\xi \quad . \tag{2.11}$$

The characteristic cluster size itself grows like a power law as p reaches p_c,

$$s_\xi(p) \propto \mid p - p_c \mid^{\frac{-1}{\sigma}}, \quad p \to p_c \quad . \tag{2.12}$$

These expressions define two extra critical exponents: τ and σ.

2.2.4 Mean cluster size

According to the results above, the probability that a chosen site belongs to any cluster of size s is $sn(s,p)$. Thus, the average cluster size is

$$\chi(p) = \frac{\sum_s s^2 n(s,p)}{\sum_s s n(s,p)} \quad . \tag{2.13}$$

By definition, the mean cluster size $\chi(p)$ does not include the percolating cluster. Thus, it decreases for $p > p_c$ because the percolating cluster leaves less space for the non-percolating ones. For $L \to \infty$, the mean cluster size diverges for $p \to p_c$ as a power law with critical exponent $-\gamma$,

$$\chi(p) \propto \mid p - p_c \mid^{-\gamma}, \quad p \to p_c^- \quad . \tag{2.14}$$

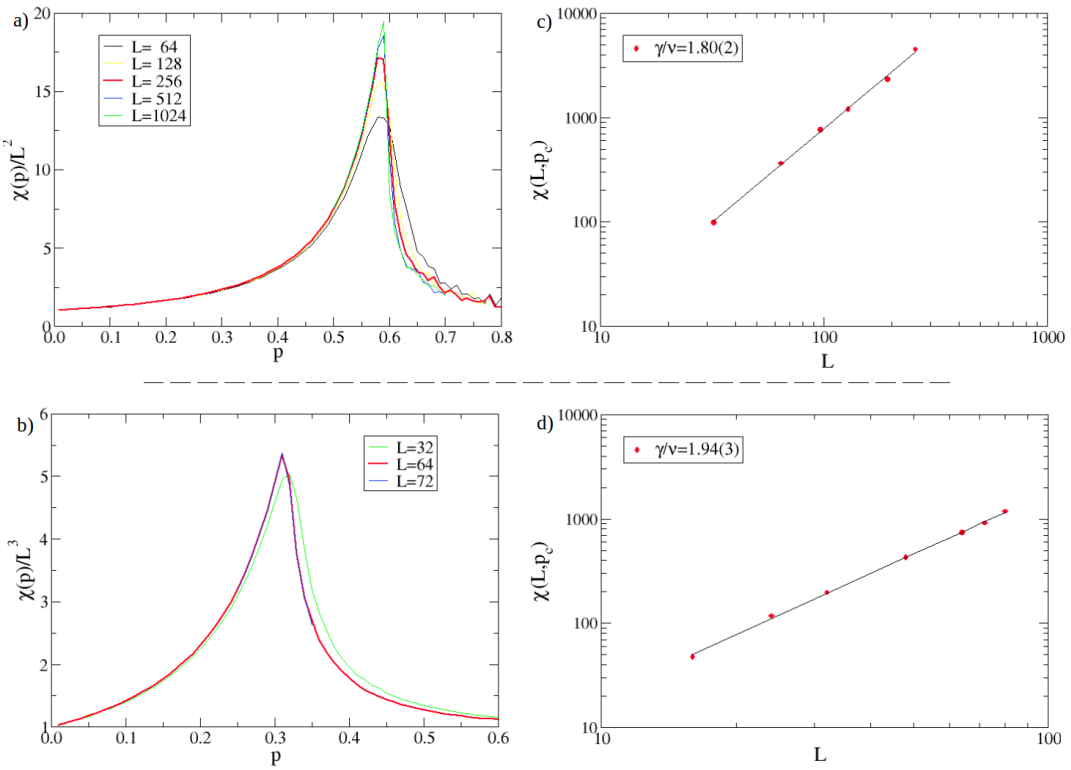

FIGURE 2.7. (left) Numerical results for the mean cluster size $\chi(L, p_c)$ for site percolation on (a) 2D and (b) 3D square lattices of several system sizes L, using the DPL algorithm (see Section 3.3). (right) Effective value of the mean cluster size at p_c against L for (c) two and (d) three dimensional systems. The slopes give $\gamma = 2.40(4)$ and $\gamma = 0.75(4)$ for two and three dimensions, respectively.

As before, applying finite-size scaling to Eq. (2.14) we get

$$\chi(p_c, L) \propto L^{\frac{\gamma}{\nu}} \quad . \tag{2.15}$$

This expression can be used to estimate γ (Fig. 2.7).

2.3 An example: site percolation in two and three dimensions

To test the algorithm we will use in our work, we estimated first the critical exponents for site percolation on square lattices in two and three dimensions (Fig. 2.2, 2.4, 2.5, 2.6, 2.7). This values are recorded in (Tab. 2.1). The agreement with the accepted values is excellent [1].

	2D		3D	
Exponents	Reported	Estimated	Reported	Estimated
p_c	0.592746(5)	0.593(5)	0.311605(5)	0.313(3)
ν	$\frac{4}{3}$	1.40(5)	0.8765(1)	0.90(6)
β	$\frac{5}{36}$	0.16(4)	0.4181(6)	0.48(5)
γ	$\frac{43}{18}$	2.40(4)	1.793(3)	1.75(4)
σ	$\frac{187}{91}$	2.0(5)	0.4522(8)	0.4(5)

TABLE 2.1. Critical exponents for square site percolation in two and three dimensions, reported [1] and estimated by using finite-size scaling [23] with the DPL algorithm (see Section 3.3).

CHAPTER 3

Percolation study of capillary rising

Consider a sandpile with its base covered with water. If grains are close enough, water will rise through the interstices of the grains, creating a liquid structure. This only happens if grains are close enough to build capillary bridges among them. There is a maximal distance among grains $S_c = 2\lambda$ a capillary bridge can overcome. As discussed in Chapter 1, this distance is determined by contact angle θ_c (in the toroidal approximation [10]) and surface tension γ (in more exact descriptions). These bridges should be connected in order to build a path for the rising water. From a theoretical point of view, it would be possible to join two bridges with a meniscus; but micro-tomographies on wet experimental random granular arrays of monodisperse spheres [3] showed that the minimal building block of the connected structure is the trimer, i.e. the junction of three liquid bridges and a meniscus [18] (Fig.1.13). These trimers, together with the volumes they eventually enclose, form a capillary path for water to rise (Fig. 1.14).

Consider a random configuration of grains. Once the positions of all grains are fixed, the possibility of building a capillary path must strongly depend on λ, i.e. the maximal half-length of a capillary bridge. If λ is too short, the places where capillary bridges and trimmers could eventually form show a disconnected structure, and water will never rise by capillarity. On the contrary, if λ is large enough, they could join together to build a percolating path. Thus, there should be a critical half-length, λ_c, at which a percolating path start to exist. From this point of view, such a path can be studied as a

pure geometrical object; it is still not filled with water, but draws the route for the water to rise. The transition for this structure from a disconnected phase to a connected one may be considered a classical percolation problem.

The aim of the present work is to characterize this transition for a random dense packing (RDP) of monodisperse spherical grains by using the standard analysis techniques of percolation theory. The study can be divided into three steps. The first step is referred to the generation of the random dense packing of spherical grains with the desired volume fraction. The second one is given by determining which void places among grains could be part of a capillary structure. The third one is the implementation of the algorithms to study the percolation of this geometrical set.

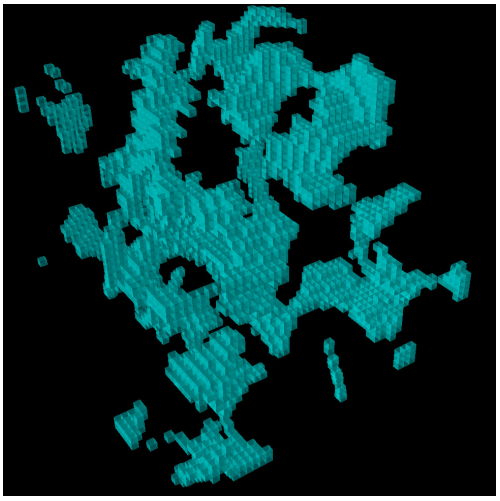

FIGURE 3.1. Three-dimensional plot of all capillary structures (bridges, trimers and enclosed volumes) in a mono-disperse sample of 87 grains with volume fraction $\phi \simeq 0.63$ at a capillary length $\lambda = 0.025R$, R the radius of the grains.

3.1 Random dense sphere packing generation

A sphere packing is an arrangement of non-overlapping spheres within a containing space. In our work we consider all spheres with the same radius R, in what is called a *monodisperse packing*. The random close packing (RCP) is the ensemble of all grain configurations with the maximal volume fraction one can obtain without crystalline subsets in it, a volume fraction that for monodisperse spheres packing is around $\phi_{RCP} = 0.64$ [50]. A random dense sphere packing (RDP) is a random sphere packing close to that maximum packing density ϕ_{RCP}.

There are many computational algorithms to generate a random dense packing of monodisperse spheres. For example, the Lubachevsky-Stillinger algorithm (LS) [51] bases on molecular dynamics simulations of elastic spheres. There are many algorithms based on LS, like the 'shaking' algorithm: A solid container is filled with grains, and the container is shaken to reduce the volume, allowing more grains to be added to the container. Other algorithms are The Jodrey-Tory algorithm [52] and the force-biased algorithm [53].

Our first try was to implement a molecular dynamics algorithm to generate the random dense packing, but this attempt was not successful. Written on $C++$ and implemented in $OpenMP$, that algorithm allowed us to simulate just 5000 particles at void fractions around $\phi = 0.59$. The algorithm, running on a computer (called $ssf1$) with 20 threads on two *Intel(R) Xeon(R) CPU E5-2695 v3* processors (see Tab. 3.1 for the detailed specifications) took between two and three days per configuration.

	Server		
Item	ssf1	ssf2	ssf3
OS	Red Hat Enterprise Linux ComputeNode release 7.3	Slackware 14.1	Slackware 14.1
CPU	2 X Intel(R) Xeon(R) CPU E5-2695 v3 @ 2.30GHz	Intel(R) Xeon(R) CPU E5-506 @ 2.13GHz	Intel(R) Core(TM) i7-4710HQ CPU @ 2.50GHz
Core(s) per socket	14	4	4
RAM	120Gb	32Gb	16Gb
GPU	2 X Tesla K40m	-	-
GPU's cores	2880	-	-
GPU's RAM	12Gb	-	-

TABLE 3.1. Basic information of the servers used in this work.

Instead, we finally decided to use a program written in $C++$ by Baranau and co-workers under open license [54] . This program uses the Jodrey-Tory (JT) algorithm to generate a random dense packing. The first step is to generate N random (the center of all spheres) inside a box of size L (Fig. 3.2). The JT algorithm is controlled by two parameters, called the outer radius and the inner radius. The first one coincides with the radius of the spherical grains and the second one takes into account an allowed overlapping distance among the grains. The algorithm progressively takes apart the overlapping spheres - starting with the two with the largest overlapped by a fixed fraction of the overlapping,

until no inner spree overlaps with another one (For more details on the algorithm, see [54]). With the JT algorithm we could get a packing density of $\phi = 0.629 \pm 0.005$ in average, up to 50000 spherical grains.

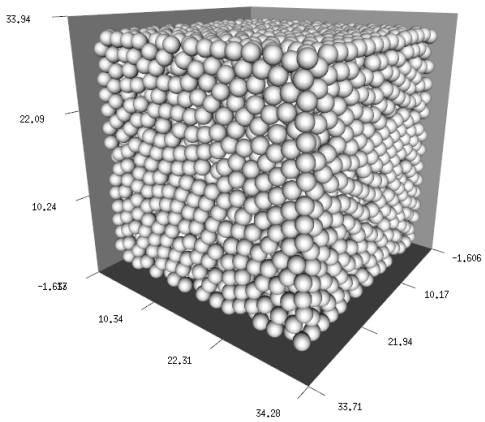

FIGURE 3.2. A random packing of 6000 monodispese spheres at a packing density $\phi \approx 0.63$, generated with the Jodrey-Tory algorithm.

Since a good statistical analysis is needed, 1000 configurations of RDP were generated for each system size L. The computational time for each configuration was between $300min$ using $ssf2$ and around $500min$ using $ssf3$ on a single core (seeTab. 3.1)). A couple of additional scripts in *bash, R* and *Python* were written to generate a configuration at each core simultaneously: 15 configurations at the $ssf1$ server, 8 configurations in two $ssf2$ servers (4 configurations each) and 12 configurations at six $ssf3$ computers (2 configurations each), reaching the simultaneous generation of 35 configurations. So, generating 1000 configurations took around 8 days. These were saved in plain text files with the positions of all grains.

3.2 Determining the potential capillary structures

The next step is to build up the capillary structures (bridges, trimers and enclosed volumes) which can form the percolating path. The problem reduces to identifying sets of two, three or four grains whose interparticle distances are below $S_c = 2\lambda$ Fig. 1.13). The basic problem was to find an efficient way of building these liquid structures, avoiding to repeat bonds between grains. For example if two grains belong to a trimer, only the structure of the trimer is built and not the liquid bridge, which in principle is already immersed into the trimer. The problem was solved by implementing three different lists of grains: pairs

of grains that can build bridges in the first list, trios of grains that can build trimers in the second one and sets of four grains that can form enclosed volumes in the third one. Next, all four trimers included in each enclosed volume were deleted from the second list. Similarly, all bridges included in a trimer or an enclosed volume were deleted from the first one. With this small algorithm it is guaranteed that liquid structures that are already contained in larger ones are not built twice, and the computational time is reduced.

Later, the system was discretized with a fine grid of cubic cells of side $a = 0.031R$, and each cell was verified to determine if it was inside a capillary structure. This procedure was implemented by using parallel programming in *bash*. In total 10 threads were used (limited by the RAM of the GPUs (12Gb each)) that allows to inspect 10 configurations at the same time (each thread is independent from the others, that means that each thread can inspect the next configuration without waiting for the other threads to finish). Reading a configuration of 40000 grains, identifying capillary structures and verifying all cells took around $20min$ using the $ssf1$ server.

3.3 Cluster labeling

The main problem in a percolation study, specially in studies based on site percolation like ours, is the large amount of data that must be labeled by clusters to obtain a good estimation of the parameters that describe the phase transition (as mentioned in Cap. 2). In order to label the cells inside the potential capillary structures, some very efficient methods were considered, including the Burning method [55], the Newman and Ziff method [56] and the Hoshen and Kopelman algorithm (HK) [57]. Initially it was decided to implement the HK algorithm. It pass through the configuration cell by cell (plane by plane, as a typewriter) searching for occupied sites. If the cell has no labeled neighbour, then a new cluster is created with a consecutive numerical label. If the cell has one occupied neighbour, then the current cell copies that label. But, if the cell has more than one neighbouring cell with a label, then it takes the label of the lowest-numbered one, and the labels of the other ones are marked as part of the cluster with the label of the cell under inspection. Because the sizes of the system to be analyzed were too large ($800 \times 800 \times 800$), the computational time to label the clusters was very long (a week per

configuration of the largest system, using $ssf1$). Thus, it was necessary to find a more efficient solution.

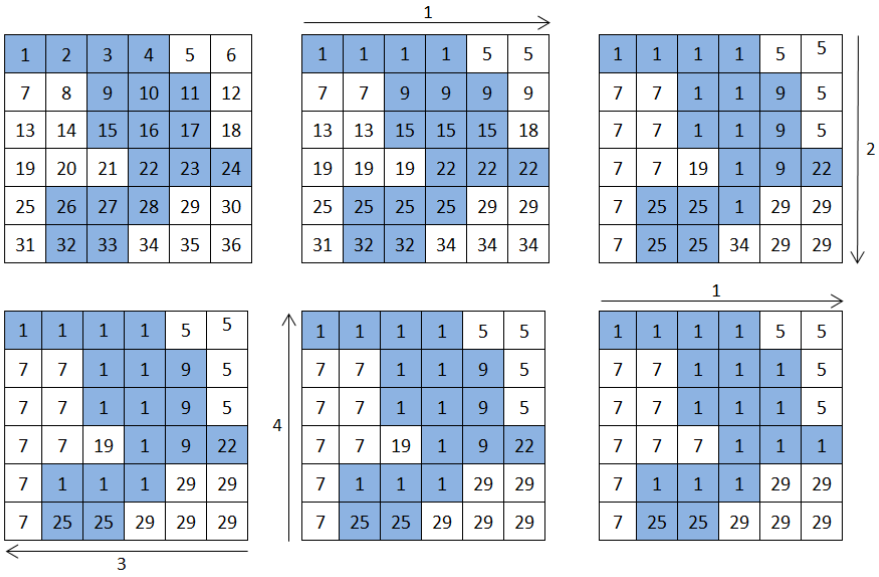

FIGURE 3.3. The Directional Propagation Label algorithm for a two dimensional array of sites (4 directions).

To solve this issue we proceeded to implement an algorithm based on the HK, but on GPUs, called Directional Propagation Labeling algorithm [58]. First, each occupied cell is labeled with a different number. Next, a cartesian axis, x, y or z, is chosen and a thread in the GPU is assigned to each row parallel to that axis. Each thread iterates through the row propagating the lowest numeric label along the row. By iteratively calling the treads on each direction (positive or negative) for each dimension, the algorithm propagates the lowest labels through the mesh (Fig. 3.3): if the cell under inspection has a higher label than the previous one, it copies that label; otherwise, the current cell keep the same label. This procedure is repeated until no more changes in the labelling are made in a whole iteration. A whole iteration counts for propagations on both directions on all axes (4 propagations in 2D and six in 3D).

This algorithm was proved by computing the critical exponents for the site percolation problem in 2D and 3D. Those values are in (Tab. 2.1). The algorithm was implemented on the server $ssf1$, which has two GPUs *NVIDIA TESLA K40m* with 2880 processor cores each (Tab. 3.1), using the programming language *CUDA*. The algorithm took around $50min$ per configuration for the largest system size considered ($L = 64$). The total com-

putational time for identifying the capillary structures and labelling the clusters for all system sizes took approximately 10 days in $ssf1$, and generated 10GB of data.

3.4 Estimation of the critical exponents

The granular medium was modeled as a dense random packing of monodisperse spheres of unitary radius with volume fraction $\phi \approx 0.63$, slightly below the random close packing. The spatial configurations of spheres were generated by using the algorithm of Jodrey and Tory [52] on cubic volumes of sizes $L = 20, 22, 26, 30, 36, 42, 48, 56$ and 64, in units of the particle radius (R), and configurations were accepted if the overlapping lengths between any two spheres was below 0.015, also in units of the particle radius. With this procedure, 1000 random configurations per size were generated for sizes $L \leq 42$ and 500 configurations per size, for sizes $L \geq 48$. That corresponds to around 1560 grains for each configuration with $L = 20$ and 38200 grains for each one with $L = 64$. For each configuration, the system was discretized with a fine grid of cubic cells of side $a = 0.031$ (we will refer to this value in a couple of lines ahead).

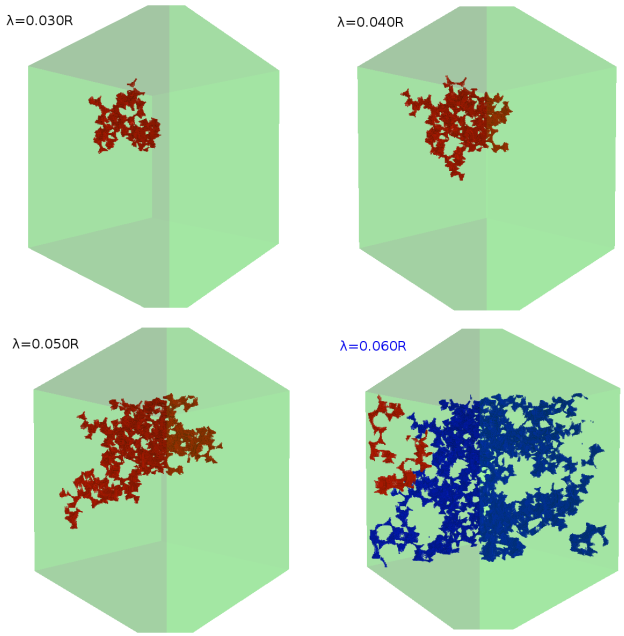

FIGURE 3.4. Potential capillary rising path (interconnected trimers and enclosed volumes) in a mono-disperse sample of 1560 grains ($L = 20R$) with radii R and volume fraction $\phi \approx 0.63$ at different values of maximal half-length λ. The percolating cluster is colored blue and the longest cluster, excluding the percolating one, is colored red.

Once a value for λ was set, each cell was checked to be part of a bridge, trimer or enclosed volume. Next, the Directional Propagation Labelling algorithm (DPL) [58], implemented on GPUs, was employed to determine if there was a percolating cluster connecting the lower and upper borders of the cube (Fig. 3.4). Finally, a bisection algorithm [59] was implemented to determine the effective critical value λ_c^{eff} where a percolating cluster first appears on that configuration. The cumulative distribution of these effective critical values for each size are the sigmoids (Fig. 3.5) that will be the incoming data for the finite-size scaling procedure that follows. The value a mentioned before is the relationship between the size of the system $L = 64$ and the number of cells considered to discretize it ($800 \times 800 \times 800$). This cell resolution was chosen because a slightly larger resolution ($820 \times 820 \times 820$) gives an effective critical half-length λ_c^{eff} between the 1% of the previous value, but takes almost twice CPU time.

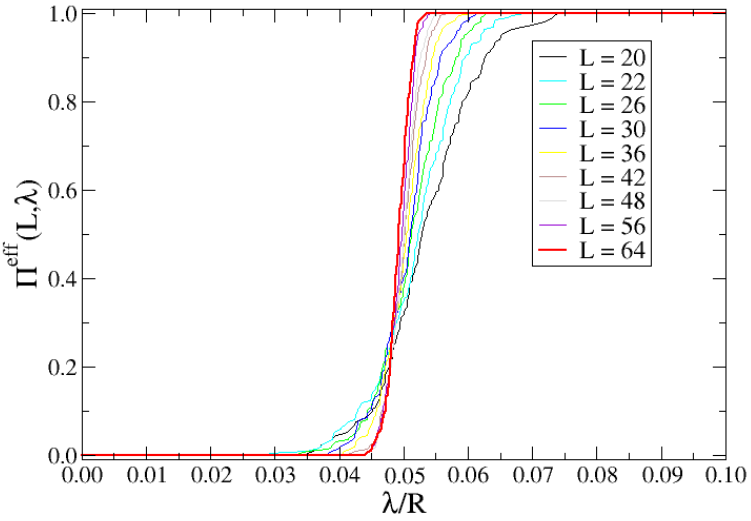

FIGURE 3.5. Probability of the capillary structure to percolate as a function of the maximal half-length of a capillary bridge λ.

The critical exponents and the critical half-length λ_c for the transition are obtained by the finite-size scaling procedure [23]. The scaling procedure starts by fitting the function given by Eq. (2.5) to the cumulative distribution of each size. The effective critical half-length $\lambda_c^{eff}(L)$ and the width $\Delta(L)$ obtained from those fittings are plotted against the system size L to obtain the critical parameters of the transition, as follows.

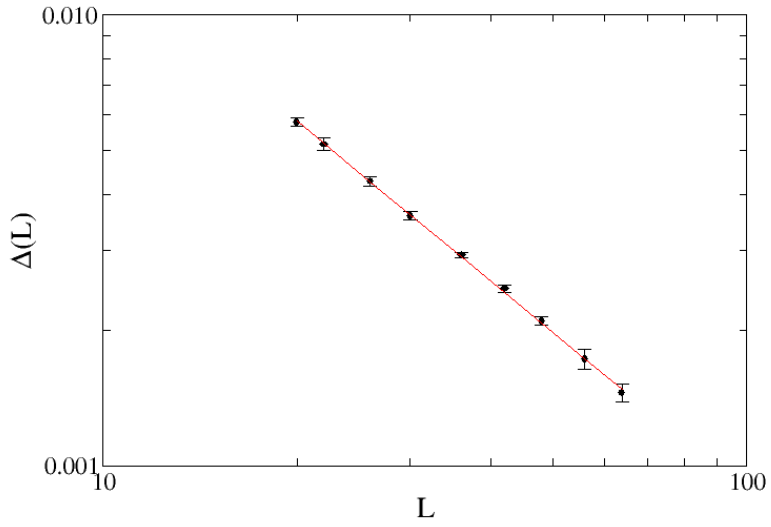

FIGURE 3.6. Width of the probability to percolate $\Delta(L)$ as a function of system size L. The line is the best power-law fit, with slope $\frac{1}{\nu} = -1.766 \pm 0.031$.

Once we have the values of $\Delta(L)$ for different sizes L, it is possible to compute the value of critical exponent ν driving the divergence of the correlation length, $\xi \propto [\lambda - \lambda_c]^{-\nu}$. Assuming the first scale relation, Eq. (2.6), and plotting $\Delta(L)$ against L (Fig 3.6), $1/\nu$ corresponds to the slope of that plot in log-log scale. Our procedure gives $\nu = 0.850 \pm 0.038$[1].

Similarly, plotting $\lambda_c^{eff}(L)$ against $L^{-1/\nu}$ (Fig 3.7) estimates the critical value λ_c for a system of infinite size, because

$$\lambda_c^{\text{eff}}(L) - \lambda_c \propto L^{-\frac{1}{\nu}} \quad . \tag{3.1}$$

The value λ_c is very important, since the next critical exponents must be calculated at this point. From Eq. (3.1) the critical value λ_c is the intercept of the linear regression of $\lambda_c^{eff}(L)$ against $L^{-1/\nu}$ with the y axis, that is the extrapolation to a system with infinite size. Our result is $\lambda_c = (0.049 \pm 0.004)R$.

Now that we have an estimation of the value λ_c it is possible to find three more critical exponents that quantify the scale-free behaviour of other three some geometric properties near the percolation threshold. Using the scaling law Eq. (2.8) and plotting the effective

[1]Here and everywhere, error bars are 1 sigma

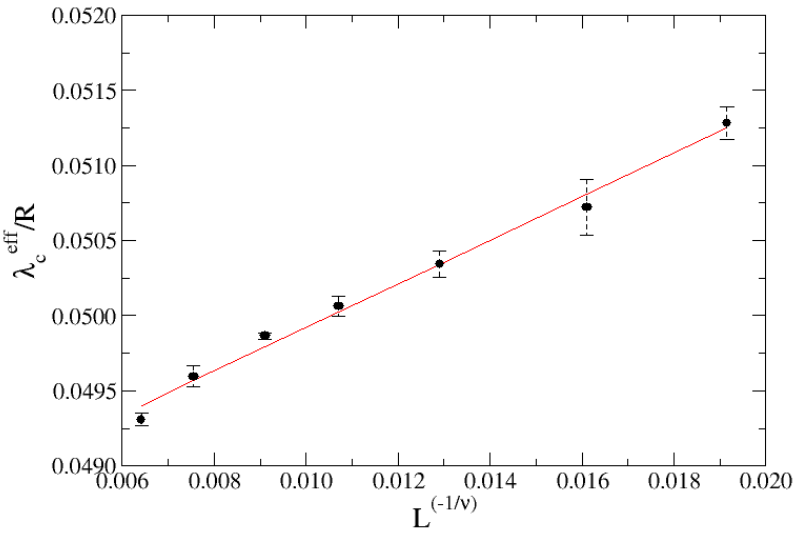

FIGURE 3.7. Effective critical half-length of a capillary bridge, $\lambda_c^{eff}(L)$, against $L^{-\frac{1}{\nu}}$. The linear fit (continuous line) estimates a cut with the vertical axis at $\lambda_c = (0.0493 \pm 0.0042)R$.

order parameter $P_\infty(L, \lambda_c)$ against L (Fig. 3.8) it is possible to find the critical exponent β, which characterizes the scale-free behaviour of the order parameter, that is the probability that a cell belongs to the percolating cluster $P_\infty(\lambda) \propto (\lambda - \lambda_c)^\beta$ for $\lambda \to \lambda_c^+$. From the slope of the fitted function in log-log scale (Fig. 3.8) we get that $\beta = 0.415 \pm 0.011$.

Also, it is possible to find the critical exponent that defines the divergence of the characteristic cluster size, σ around λ_c as $s_\xi(\lambda) \propto \mid \lambda - \lambda_c \mid^{\frac{-1}{\sigma}}$ (Eq. (2.12) and Fig. 3.9). The slope for the effective characteristic cluster size as a function of the system size in log-log scales (Fig. 3.9) $D = 1/\sigma\nu = 2.9 \pm 0.3$ is known as the fractal dimension of the system, from where we can obtain $\sigma = 0.406 \pm 0.042$.

Finally we find ω, the critical exponent of the mean cluster volume $V(\lambda)$, which close to the percolation threshold goes like $V(L, \lambda_c) \propto L^{\frac{\omega}{\nu}}$. This exponent can be calculated from the slope of function that relates the effective mean cluster volume with the system size in log-log scale (Fig. 3.10). Our result is $\omega = -0.26 \pm 0.09$. The negative value of this exponent can be explained by the fact that we are considering the bridges in our construction. Scheel and co-workers show by experimental measurements [3] that in liquid structures of this type there are more isolated bridges than connected clusters, i.e. the mean cluster volume tends to the average value of the bridges' volumen.

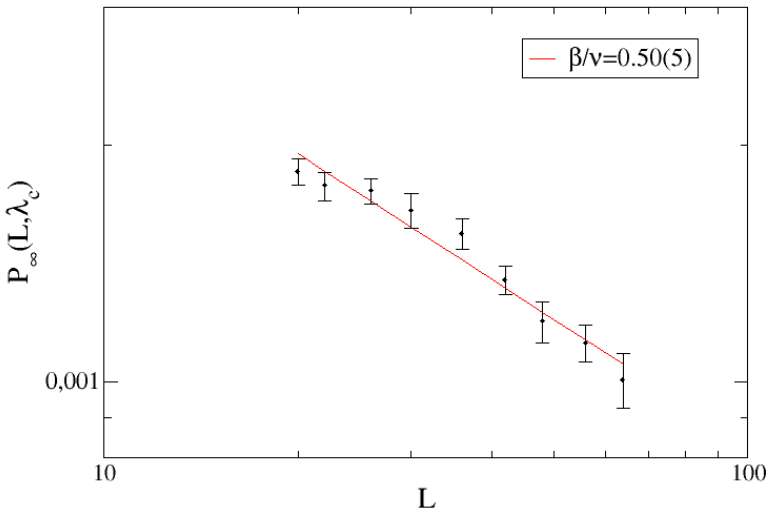

FIGURE 3.8. Effective value of the order parameter at λ_c against L. The slope gives $\beta = 0.415 \pm 0.011$.

Tab. 3.2 summarizes the values of all computed critical exponents, compared with the exponents for normal site percolation in three dimensions. This concludes our percolation study of capillary rising

Exponents	Capillary rising	3D site percolation	Difference (%)
ν	0.850 ± 0.038	0.8765(1)	3.0
β	0.415 ± 0.011	0.4181(6)	0.7
σ	0.406 ± 0.042	0.4522(8)	10.2
D	2.9 ± 0.3	2.5226(1)	15.0
ω	-0.26 ± 0.03	-	-

TABLE 3.2. Comparison between the critical exponents of our model of discrete capillary rising and normal site percolation.

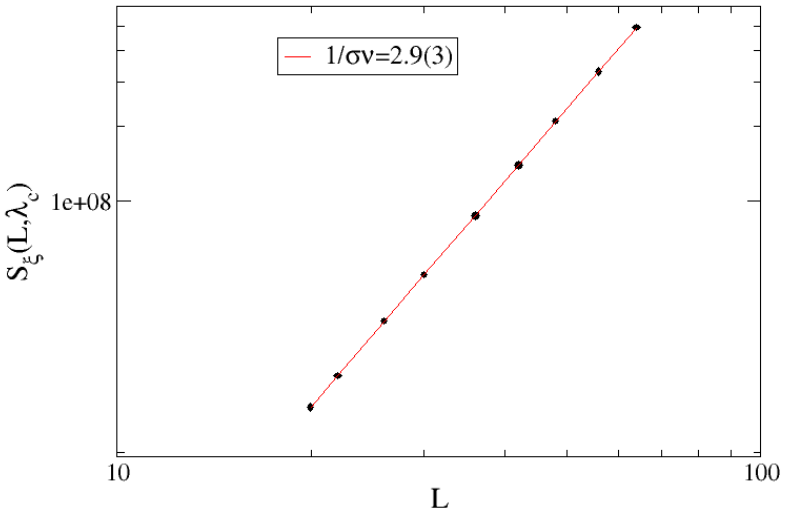

FIGURE 3.9. Effective characteristic cluster size at λ_c against L. The slope gives $\sigma = 0.406 \pm 0.042$.

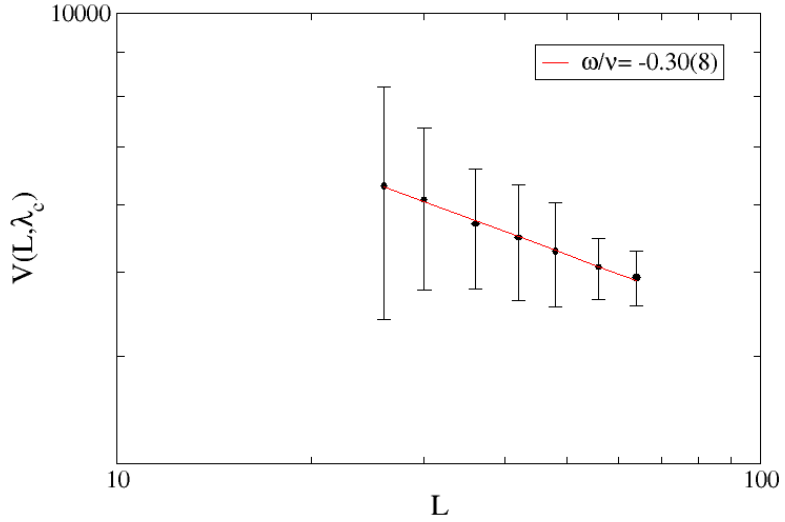

FIGURE 3.10. Effective mean cluster volume at λ_c against L. The slope gives $\omega = -0.26 \pm 0.09$.

4

Conclusions

Consider a granular media where grains are so closed that water can rise between them by capillary forces. This work investigated how the spaces in the pores that eventually could be part of capillary structures like bridges, trimers and enclosed volumes can join together to form a connected path at disposal for capillary rising. The control parameter we chose to drive such a transition is the maximal length of a capillary bridge, a function of the contact angle that can be modified in real soils through the use of hydrofobants. The study has been conducted for random dense packings of monodisperse spherical grains as a first prototyping model of granular materials, and the analysis has been performed with the classical finite size scaling techniques of percolation theory.

The finite-size scaling we obtained is of very good quality (Figs. 3.6, 3.8, 3.9 and 3.10), suggesting that the percolation theory fits well the problem and that there is, indeed, a phase transition guided by the maximal length of a capillary bridge. For packings at volume fraction $\phi \simeq 0.63$, our results show that the transition to a connected structure occurs at a maximal length of a capillary bridge $2\lambda_c = (0.098 \pm 0.008)R$, less than one half of the mean distance between neighbouring grains in the samples at that volume fraction (around $(0.258 \pm 0.007)R$). This indicates that a connected path for capillary rising appears much easier than expected if one just look at the distances among grains. In addition, the exponents we obtained for the order parameter (β), the correlation length (ν), the effective characteristic cluster size σ and the fractal dimension at criticality D are compatible to those of size percolation in three dimensions (as illustrated in Tab. 3.2). This result suggests that facets among three neighbouring grains could turn into trimers

which are actually the basic building blocks of the path for capillary rising at disposal for the capillary rising almost independently from each other, a possible consequence of the random positions for the grains. This similarities imply that the two systems belong to the same universality class. Thus, the setting of a connected path at disposal for capillary rising shows to be driven by three-dimensional site percolation.

One more critical exponent that can be computed to verify the result above is γ, the critical exponent driving the divergence of the average cluster size. Since the basic unit to build a path for capillary rising is the trimer, such computation should account for the mean number of trimers in a cluster. Similarly, it would be worth to reproduce the present study for other void fractions to determine how general our conclusions are. These are both interesting topics for future works. Also, a usual way to control capillary rising, as we mentioned before, consists in treating some part of the grains with hydrophobic solutions that alter the contact angle, reducing 2λ. The key question that we want to answer in future works is which proportion of the material has to be treated to avoid capillary rising. To response that question, the simulation can proceed in a similar way as the present one, but with three different maximal half maximal lengths λ: one between untreated grains, other between treated grains and a third one between one treated and one untreated grain. Such a future work will be of great interest in geotechnics and related studies.

The present study combines capillary structures and percolation theory to investigate capillary rising through a granular medium. It constitutes an interesting novel approach and a new step in the understanding of this rich phenomenon.

APPENDIX A

Powders and Grains 2017

Part of this work has been accepted and will be presented at the 8th International Conference on Micromechanics of Granular Media (*Powders and Grains 2017*), which will be held in Montpellier, France, on July 3-7, 2017. The submitted paper is the following:

Percolation study for the capillary ascent of a liquid through a granular soil

Manuel Antonio Cárdenas-Barrantes[1,⋆], *José Daniel* Muñoz[1,⋆⋆], and *Nuno Machado* Araujo[2,⋆⋆⋆]

[1] *Simulation of Physical Systems Group, Department of Physics, Universidad Nacional de Colombia, Carrera 30 No. 45-03, Ed. 404, Of. 348, Bogota D.C., Colombia.*

[2] *Centro de Física Teórica e Computacional, Departamento de Física, Faculdade de Ciências, Universidade de Lisboa, Campo Grande, P-1749-016 Lisboa, Portugal.*

Abstract. Capillary rise plays a crucial role in the construction of road embankments in flood zones, where hydrophobic compounds are added to the soil to suppress the rising of water and avoid possible damage of the pavement. Water rises through liquid bridges, menisci and trimers, whose width and connectivity depends on the maximal half-length λ of the capillary bridges among grains. Low λs generate a disconnect structure, with small clusters everywhere. On the contrary, for high λ, create a percolating cluster of trimers and enclosed volumes that form a natural path for capillary rise. Hereby, we study the percolation transition of this geometric structure as a function of λ on a granular media of monodisperse spheres in a random close packing. We determine both the percolating threshold $\lambda_c = (0.049 \pm 0.004)R$ (with R the radius of the granular spheres), and the critical exponent of the correlation length $\nu = 0.830 \pm 0.051$, suggesting that the percolation transition falls into the universality class of ordinary percolation.

1 Introduction

Consider a sandpile with its base covered with water. If grains are close enough, water will rise through the interstices of the grains. This capillary rise plays a major role in the transport of fluids across porous media, including water and oil wells. Specially in unsaturated soil structures, like embankments, the capillary rise of water is a real concern, because water can damage the integrity of the structure [1]. The broad spectrum of possible solutions include the use of hydrophobic materials [1] or even the addition of active mechanisms to compensate for the deformations produced by capillary forces [2].

The rising of water through a granular medium is strongly determined by the geometry of the interconnected structure of pores among the grains. First models [3] represented that structure by sites (pore bodies) of arbitrary shape and position interconnected by bonds (pore throats), whose sizes and shapes could be obtained from experimental probes [4, 5]; many properties, like relative permeability [6] or drainage and imbibition [7] can be estimated from this simplified model. More recent works focus on representing the liquid structures among grains (bridges, menisci and pore bodies) as real as possible, based on experiments (as in X-Ray microtomography [8]) or in computer simulations [9, 10]. This modeling is able to reproduce water saturation and drying with the water volume as control parameter and to compute forces and pressures [10]. Together with experiments, they have succeeded identifying trimers (that is, the junction of three liquid bridges and a meniscus) as the minimal building block to build a pathway for rising water [8, 10]. The structure itself must strongly change with the critical length of a capillary bridge (a function of contact angle and surface tension [11]), and some studies in two dimensions have been performed to find when a connected structure first appears as either the contact angle [12] or the liquid volume [13, 14] increases.

The present work investigates how the set of trimers and enclosing pore bodies at disposal for capillary rising changes from a fully disconnected structure to a connected pathway as the critical length of the capillary bridges increases. The goal is to find both the critical half-length λ_c for the transition and the critical exponent ν for the correlation length. The study is performed on the interstices on three-dimensional random close packings of monodisperse spheres. The capillary model of trimers and pore bodies on random close packings is introduced in Sec. 2. Next, Sec. 3 analyses the resulting capillary structures by using tools of percolation theory [15–17]. Finally, Sec. 4 summarizes the main conclusions and discussions.

2 Capillary model

From a microscopic point of view, water can rise if the grains are close enough to build capillary bridges among them. The shape of a capillary bridge between two identical spherical grains is not strongly affected by gravity, but determined by the contact angle θ_c, the liquid-gas surface tension γ, the liquid volume V and the distance S between

⋆ e-mail: macardenasb@unal.edu.co
⋆⋆ e-mail: jdmunozc@unal.edu.co
⋆⋆⋆ e-mail: nmaraujo@fc.ul.pt

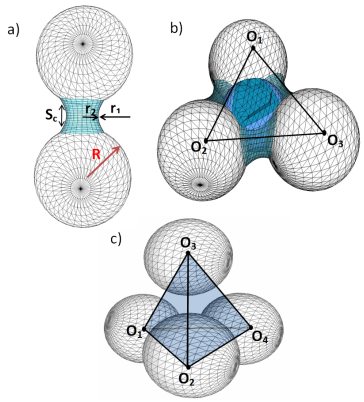

Figure 1. Main capillary structures. (a) Liquid bridge with separation distance S. (b) Trimer, built by three liquid bridges (light blue) and a meniscus (dark blue). (c) A liquid volume enclosed by four trimers.

the grains [18]. There is a maximal distance among grains $S_c = 2\lambda$ a capillary bridge can overcome. If $S < 2\lambda$, a capillary bridge may eventually established for some V; otherwise, there is no possible path between the grains for the water to rise. This limit can be estimated through the toroidal approximation method [19] (Fig. 2) or by numerical simulations.

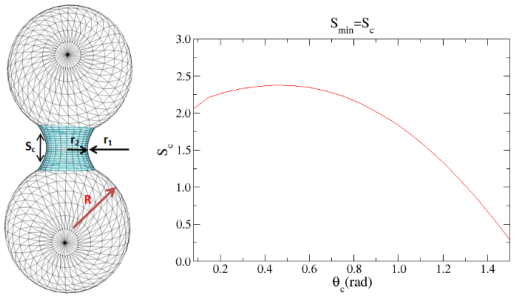

Figure 2. (a) Liquid bridge with separation distance S. (b) Maximal separation distance S_c for a capillary bridge as function of the contact angle θ in the toroidal approximation (deduced from data in [11]).

The bridges among grains should be connected in order to build a path for the rising water. From a theoretical point of view, it would be possible to join two bridges with a meniscus; but micro-tomographies on experimental random granular arrays of monodisperse spheres [8] do not show that kind of structure. On the contrary, the minimal connected structures are trimers, that are the junction of three liquid bridges and a meniscus [10] (Fig. 1). A trimer will eventually form for some water content if three grains are so close together that the distances between any two of them are shorter than S_c and the angles between every two bridges are smaller than $\pi - 2\theta_c$ [11]. Two trimers are assumed connected if they share a bridge, and connected trimers can eventually enclose filling volumes (Fig. 1). Trimers and enclosed volumes form the structure for capillary rising. If S_c is small, the structure is a disconnected set of clusters. On the contrary, if S_c is large enough, there is a connected path across the sample, i.e. a percolating passage for the liquid to rise. The aim of the present work is to characterize the transition across these two regimes - driven by λ, the half maximal length of a capillary bridge - on a monodisperse set of spherical grains by using the standard tools of classical percolation.

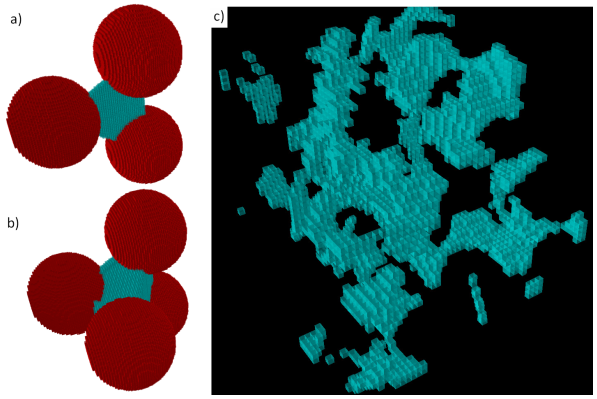

Figure 3. a) Triangle-like liquid structure (trimer). b) Tetrahedron-like liquid structure (enclosed volume). c) Potential capillary rising path (interconnection trimers and enclosed volumes) in a mono-disperse sample of 87 grains with volume fraction $\phi \simeq 0.63$ at a capillary length $\lambda = 0.025R$, R the radius of the grains (The curve contour do not come from the exact shape of trimers and menisci, but from the removed grains).

3 Procedure and Results

The granular medium was modeled as a dense random packing of monodisperse spheres of unitary radius with volume fraction $\phi \approx 0.63$, slightly below the random close packing [20]. The spatial configurations of spheres were generated by using the algorithm of Jodrey and Tory [21] on cubic volumes of sizes $L = 22, 26, 30, 36, 42, 48, 56$ and 64, and configurations were accepted if the overlapping lengths between any two spheres was below 0.015, in units of particle radius. With this procedure, 200 configurations per size for sizes $L \leq 42$ and 500 configurations per size for sizes $L \geq 48$ were generated, corresponding to around 1560 grains each for $L = 22$ and 38200 grains each for $L = 64$.

For each configuration, we identify sets of three and four grains whose interparticle distances are below $S_c = 2\lambda$, and we built triangle-like (trimer) and tetrahedron-like (enclosed volume) structures with those sets of three or four grains, respectively (Fig. 3). The space occupied by the grains themselves is removed. The interconnection of those structures corresponds to possible capillary rising paths. Single bridges are not included, because they are not observed in experiments to contribute to the percolating structure, as discussed in the previous section. The actual shape of the capillary bridges and menisci are not included, because only the connectivity among elements

is relevant for the percolation exponents, and not the detailed shape of the percolating elements themselves [15]. Then, the whole structure is discretized with a fine grid of cubic cells of side $a = 0.031$. Once a value for λ was set, each cell was checked to be part of a trimer or an enclosed volume, and trimers become a couple of cells thick. By doing so, the volume that can be occupied by the liquid phase appears as a discrete set of small cubes, as shown in Fig. 3. This allow us to run an efficient site percolation algorithm to study the percolation transition. Two cells are said to be part of the same cluster if they are first neighbors. The Directional Propagation Labelling algorithm (DPL) for GPUs [22] was employed to determine if there was a percolating cluster connecting the lower and upper borders of the cube. It was necessary to implement this algorithm for GPUs because the systems were very large ((800×800×800) cells for $L = 64$) and the procedure becomes very time demanding. For instance, the more traditional algorithm by Hoshen and Kopelman [23] takes around 6 hours on a CPU (Intel(R) Xeon(R) CPU E5-2695 v3 - 2.30GHz) to evaluate percolation and classify the cluster sizes for a single configuration of system size L=36. By contrast, the DPL algorithm takes only around 15 min to analyze the same configuration on an Nvidia(R) Tesla(R) K40, what is 25 times faster. The savings in computational time are even larger for larger system sizes. Finally, a bisection algorithm [24] was implemented to determine the effective critical value λ_c^{eff} where a percolating cluster first appears on that configuration. The cumulative distribution of these effective critical values for each size are the sigmoids (Fig. 4) that will be the incoming data for the finite-size scaling procedure that follows.

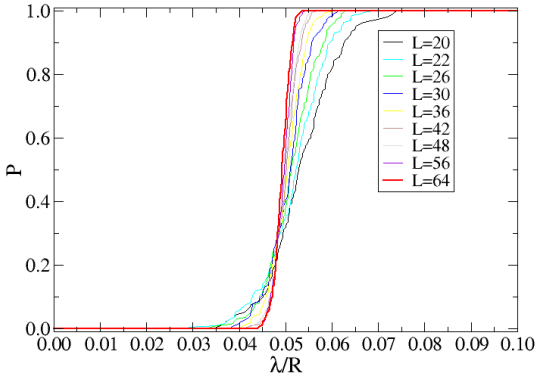

Figure 4. Probability of the capillary structure to percolate as a function of the maximal half-length of a capillary bridge λ.

The critical exponents and the critical half-length λ_c for the transition are obtained by the finite-size scaling procedure proposed by Rintoul and Torquato [25]. The scaling procedure starts by fitting the function

$$f(\lambda_c^{eff}, \Delta(L)) = [1 + \tanh[(\lambda - \lambda_c^{eff}(L))/\Delta(L)]]/2 \quad (1)$$

to the cumulative distribution of each size. The effective critical half-length $\lambda_c^{eff}(L)$ and the width $\Delta(L)$) of the distribution obtained from those fittings are plotted against the system size L to obtain the critical parameters of the transition. Assuming that

$$\Delta(L) \propto L^{\frac{1}{\nu}} \quad , \quad (2)$$

and plotting $\Delta(L)$ against L (Fig 5) gives the critical exponent ν driving the divergence of the correlation length, $\xi \propto [\lambda - \lambda_c]^{-\nu}$. We obtain $\nu = 0.830 \pm 0.051$. Similarly, plotting $\lambda_c^{eff}(L)$ against $L^{-1/\nu}$ (Fig 6) estimates the critical value λ_c for a system of infinite size, because

$$\lambda_c^{\text{eff}}(L) - \lambda_c \propto L^{-\frac{1}{\nu}} \quad . \quad (3)$$

Our result is $\lambda_c = (0.049 \pm 0.004)R$.

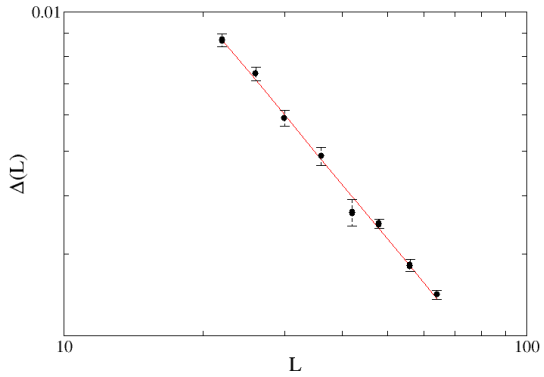

Figure 5. Width of the probability to percolate $\Delta(L)$ as a function of system size L. The line is the best power-law fit, with slope $\frac{1}{\nu} = -1.205 \pm 0.038$.

4 Conclusions and Discussions

This work investigates the capillary ascent of a liquid through a granular soil as a percolation transition driven by the half maximal distance between two grains that can be overpassed by a capillary bridge, λ. Below a critical value λ_c the structure of trimers and enclosed volumes is disconnected, and no water can rise. Above, the water percolates trough the sample. By using standard techniques of percolation analysis, we found $\lambda_c = (0.049 \pm 0.004)R$ and a critical exponent for the correlation length $\nu = 0.830 \pm 0.051$. These results deserve some discussion. First, the finite-size scaling is of very good quality (Fig. 5), suggesting that the technique fits the problem and that there is, indeed, a phase transition. Second, the critical length of a bridge, $2\lambda_c = 0.098(6)R$, is less than one half of the mean distance between neighboring grains in the samples (around $(0.258 \pm 0.007)R$) for a volume fraction $\phi \simeq 0.63$), which can be considered as a naive *a priori* estimation of such parameter. Third, the critical exponent ν is, within error bars,

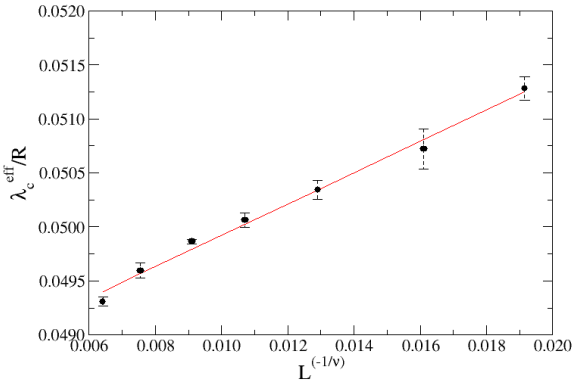

Figure 6. Effective critical half-length of a capillary bridge length $\lambda_c^{eff}(L)$ against $L^{-\frac{1}{\nu}}$. The linear fit (continuous line) estimates a cut with the vertical axis at $\lambda_c = (0.049 \pm 0.004)R$.

the one of ordinary percolation ($\nu = 0.87619(12)$ [26]). This result suggests that each facet among three neighboring grains could turn into a trimer at disposal for the capillary rising almost independently from the other facets, a consequence of the random positions for the grains. This similarity should be confirmed by computing other critical exponents, like the critical exponent β for the order parameter, which would be the probability of a cell to belong to the percolating cluster, as usual. Similarly, our study could be reproduced for other void fractions to determine how general are our conclusions. All these are thema for future works.

An usual way to control capillary rising, as we mentioned before, consists in treating some part of the grains with hydrophobic solutions that alter the contact angle, reducing λ (Fig. 2). The key question here is which proportion of the material has to be treated to avoid capillary rising. The simulation would proceed in a similar way as the present one, but with three maximal lenghts λ: one between untreated grains, other between treated grains and a third one between one treated and one untreated grain. Such a future work will be of great interest in geotechnique.

The present study combines capillary structures and percolation theory to investigate capillary rising through a granular medium. It constitutes a novel approach and a new step in the understanding of this rich phenomenon.

Acknowledgments

We thanks COLCIENCIAS Young Researchers Program, Grant 2014-645, the Universidad Nacional de Colombia and the Portuguese Foundation for Sciences and Technology (FCT) under Contracts nos. UID/FIS/00618/2013, EXCL/FIS-NAN/0083/2012, and IF/00255/2013 for finnancial support.

References

[1] N. Khalili, A. Russell, E. Khoshghalb, A, *Unsaturated soils : research and applications*, 1st edn. (Crc Press, 2014)
[2] A. Pozzato, A. Tarantino, Unsaturated Soils: Research and Applications **2**, 1082 (2014)
[3] I. Fatt, Trans AIME **207**, 144 (1956)
[4] H. Vogel, K. Roth, Advances in Water Resources **24**, 233 (2001)
[5] M. Coles, P. Hazlett, W. Soll, E. Muegge, K. Jones, Journal of Petroleum Science and Engineering **19**, 55 (1998)
[6] U. Fischer, M. Celia, Water Resour. Res. **6**, 1089 (1999)
[7] G. Mason, D. Mellor, Journal of Colloid and Interface Science **176**, 214 (1995)
[8] M. Scheel, R. Seemann, M. Brinkmann, M. Di Michiel, A. Sheppard, B. Breidenbach, S. Herminghaus, Nature Materials **7**, 189 (2008)
[9] S. Motealleh, M. Ashouripashaki, D. DiCarlo, S. Bryant, Transport in Porous Media **99**, 581 (2013)
[10] K. Melnikov, R. Mani, F. Wittel, M. Thielmann, H. Herrmann, Cond-mat. Soft **92** (2015)
[11] D. Megias-Alguacil, L. Gauckler, AlChE **55** (2009)
[12] N. Martys, M. Robbins, Phys. Rev. Lett. **66**, 1058 (1991)
[13] M. Cieplak, O. Robbins, Phys. Rev. Lett. **60**, 2042 (1988)
[14] B. Berkowitz, I. Balberg, Water Resources Research **29**, 775 (1993)
[15] D. Staufer, A. Abarony, *Introduction to percolation theory*, 2nd edn. (Taylor and Francis, 1994)
[16] M. Sahimi, *Applications of Percolation Theory*, 1st edn. (Taylor & Francis, UK, 1994)
[17] N. Araujo, P. Grassberger, B. Kahng, K. Schrenk, R. Ziff, The European Physical Journal Special Topics **223**, 2307 (2014)
[18] G. Lian, *Computer simulation of moist agglomerate colisions* (Doctoral Thesis, The University of Aston in Birmingham, 1994)
[19] R. Fisher, J. of Agricultural Science **16**, 492 (1926)
[20] M. Shahinpoor, Powder Technology **25**, 163 (1980)
[21] J. Jodrey, E. Tory, Physical Review A **32** (1985)
[22] K. Hawick, A. Leist, D. Playne, Parallel Computing **36**, 655 (2010)
[23] J. Hoshen, R. Kopelman, Phys. Rev. B **14**, 3438 (1976)
[24] W. Press, S. Teukoisky, W. Vetterlingand, B. Flannery, *Numerical recipes*, 3rd edn. (Cambridge, 2007)
[25] M. Rintoul, S. Torquato, J. Phys. A: Math. Gen. **30**, 585 (1997)
[26] X. Xu, J. Wang, J. Lv, Y. Deng, Frontiers of Physics **9**, 113 (2014)

Bibliography

[1] K. Christensen and N. Moloney, *Comlexity and Critically*. Imperial College London, UK, 1 ed., 2005.

[2] P. Gennes, F. Brochard-Wyart, and D. Quéré, *Capillarity and Wetting Phenomena*. Springer, 1 ed., 2004.

[3] M. Scheel, R. Seemann, M. Brinkmann, M. Di Michiel, A. Sheppard, B. Breidenbach, and S. Herminghaus, "Morphological clues to wet granular pile stability," *Nature Materials*, vol. 7, p. 189, 2008.

[4] K. Christensen, *Percolation Theory*. Imperial College London, 1 ed., 2002.

[5] N. Khalili, A. Russell, and E. Khoshghalb, A, *Unsaturated soils : research and applications*. Crc Press, 1 ed., 2014.

[6] A. Pozzato and A. Tarantino, "Characterisation of the hydraulic behaviour of coarse-grained flood embankment materials," *Unsaturated Soils: Research and Applications*, vol. 2, p. 1082, 2014.

[7] I. Fatt, "The network model of porous media," *Trans AIME*, vol. 207, p. 144, 1956.

[8] H. Vogel and K. Roth, "Quantitative morphology and network representation of soil pore structure," *Advances in Water Resources*, vol. 24, no. 34, p. 233, 2001.

[9] M. Coles, P. Hazlett, W. Soll, E. Muegge, and K. Jones, "Pore level imaging of fluid transport using synchrotron x-ray microtomography," *Journal of Petroleum Science and Engineering*, vol. 19, no. 12, p. 55, 1998.

[10] U. Fischer and M. Celia, "Prediction of relative and absolute permeabilities for gas and water from soil water retention curves using a pore-scale network model," *Water Resour. Res.*, vol. 6, no. 3, p. 1089, 1999.

[11] G. Mason and D. Mellor, "Simulation of drainage and imbibition in a random packing of equal spheres," *Journal of Colloid and Interface Science*, vol. 176, no. 1, p. 214, 1995.

[12] A. Hunt, R. Ewing, and B. Ghanbarian, *Percolation Theory for Flow in Porous Media*. Springer, 3 ed., 2014.

[13] M. Sahimi, "Flow phenomena in rocks from continuum models to fractals, percolation, cellular automata, and simulated annealing," *Rev. Mod. Phys.*, vol. 65, p. 1393, 1993.

[14] Y. Bernabe and C. Bruderer, "Effect of the variance of pore size distribution on the transport properties of heterogeneous networks," *J. Geophys. Res.*, vol. 103, p. 513, 1998.

[15] A. Hunt, "Percolative transport and fractal porous media," *Chaos Solitons & Fractals*, vol. 19, p. 309, 2004.

[16] R. Larson, L. Scriven, and H. Davis, "Percolation theory of residual phases in porous media," *Nature*, vol. 268, p. 409, 1977.

[17] S. Motealleh, M. Ashouripashaki, D. DiCarlo, and S. Bryant, "Unified model of drainage and imbibition in 3d fractionally wet porous media," *Transport in Porous Media*, vol. 99, no. 2, p. 581, 2013.

[18] K. Melnikov, R. Mani, F. Wittel, M. Thielmann, and H. Herrmann, "Grain scale modeling of arbitrary fluid saturation in random packings," *Cond-mat. Soft*, vol. 92, 2015.

[19] D. Megias-Alguacil and L. Gauckler, "Capillary forces between two solid spheres linked by a concave liquid bridge: Regions of existence and forces mapping," *AlChE*, vol. 55, 2009.

[20] N. Martys and M. Robbins, "Critical phenomena in fluid invasion of porous media," *Phys. Rev. Lett.*, vol. 66, p. 1058, 1991.

[21] M. Cieplak and O. Robbins, "Dynamical transition in quasistatic fluid invasion in porous media," *Phys. Rev. Lett.*, vol. 60, p. 2042, 1988.

[22] B. Berkowitz and I. Balberg, "Percolation theory and its application to groundwater hydrology," *Water Resources Research*, vol. 29, p. 775, 1993.

[23] D. Stauffer and A. Aharony, *Introduction to percolation theory.* Taylor and Francis, 2 ed., 1994.

[24] M. Rintoul and S. Torquato, "Precise determination of the critical threshold and exponents in three-dimensional continuum percolation model," *J. Phys. A: Math. Gen.*, vol. 30, p. 585, 1997.

[25] N. Araujo, P. Grassberger, B. Kahng, K. Schrenk, and R. Ziff, "Recent advances and open challenges in percolation," *The European Physical Journal Special Topics*, vol. 223, p. 2307, 2014.

[26] H. Butt, K. Graf, and M. Kappl, *Physics and Chemistry of Interfaces.* Wiley-VCH, 1 ed., 2003.

[27] R. Narayanan and E. Schwabe, D, *Interfacial Fluid Dynamics and Transport Processes.* Springer, 1 ed., 2003.

[28] E. Zandi, I, *Advances in Solid-Liquid Flow in Pipes and its Applications.* Pergamon Press, 1 ed., 1971.

[29] F. A. L. Dullien, *Porous Media, Fluid transport and pore structure.* Academic Press INC., 2 ed., 1992.

[30] A. W. Adamson and A. P. Gast, *Physical Chemistry of Surfaces*. John Wiley INC., 6 ed., 1997.

[31] G. Lian, *Computer simulation of moist agglomerate colisions*. Doctoral Thesis, The University of Aston in Birmingham, 1994.

[32] F. Bashforth and J. Adams, "An attempt to test the theories of capillary action," *University Press, Cambridge, England*, 1883.

[33] J. Strutt, "Capillarity," *Proc. Roy. Soc. London*, vol. 92, no. 2, p. 184, 1915.

[34] J. Lane, "Colloid interface sci," *UK*, vol. 42, p. 145, 1973.

[35] R. Fisher, "On the capillary forces in an ideal soil," *J. of Agricultural Science*, vol. 16, p. 492, 1926.

[36] D. Megias and L. Gauckler, "Accuracy of the toroidal approximation for the calculus of concave and convex liquid bridges between particles," *Granular Matter*, vol. 13, p. 487, 2011.

[37] D. Mazzone, G. Tardos, and R. Pfeffer, "The effect of gravity on the shape and strength of a liquid bridge between 2 spheres," *J Colloid Interface Sci.*, vol. 113, p. 544, 1986.

[38] M. Meurisse and M. Querry, "Squeeze effects in a flat liquid bridge between parallel solid surfaces," *J Tribol*, vol. 128, p. 575, 2006.

[39] G. Lian, C. Thornton, and M. Adams, "A theoretical study of the liquid bridge forces between two rigid spherical bodies," *J of Colloid and Interface Science*, vol. 161, p. 138, 1993.

[40] G. Mason and W. Clark, "Liquid bridges between spheres," *Chemical Engineering Science*, vol. 20, p. 859, 1965.

[41] M. Kohonen, D. Geromichalos, M. Scheel, C. Schier, and S. Herminghaus, "On capillary bridges in wet granular materials," *Physica A*, vol. 339, p. 7, 2004.

[42] S. Broadbent and J. Hammersley, "Percolation processes," *Mathematical Proceedings of the Cambridge Philosophical Society*, vol. 53, p. 629, 1957.

[43] S. Motealleh, *Mechanistic study of menisci motion within homogeneously and heterogeneously wet porous media*. Doctoral Thesis, The University of Texas at Austin, 2009.

[44] M. Sahimi, *Applications of Percolation Theory*. Taylor & Francis, UK, 1 ed., 1994.

[45] P. King, S. Buddyrev, N. Dokholyan, S. Havlia, Y. Lee, and G. Paul, "Applications of statistical physics to the oil industry," *Physica A*, vol. 274, p. 60, 1999.

[46] R. Cohen, D. Avraham, and S. Havlin, "Percolation critical exponents in scale-free networks," *Phys. Rev. E*, vol. 66, 2002.

[47] G. Grimmett, *Percolation*. Springer, 2 ed., 1999.

[48] J. Essan, "Percolation theory," *Rep. Prog. Phys.*, vol. 43, 1980.

[49] M. Levinshtein, B. Shklovskii, M. Shur, and A. Efros, "The relation between the critical exponents of percolation theory," *Sov. J. of Exp. and Theo. Phys.*, vol. 42, p. 197, 1976.

[50] H. Jaeger and S. Nagel, "Physics of granular states," *Science*, vol. 255, p. 1524, 1992.

[51] B. Lubachevsky and F. Stillinger, "Geometric properties of random disk packings," *J. Stat. Phys.*, vol. 60, 1990.

[52] J. Jodrey and E. Tory, "Computer simulation of close random packing of equal spheres," *Physical Review A*, vol. 32, no. 4, 1985.

[53] J. Mościński, M. Bargiel, Z. Rycerz, and P. Jacobs, "The force-biased algorithm for the irregular close packing of equal hard spheres," *Molecular Simulation*, vol. 3, p. 201, 1989.

[54] V. Baranau, D. Hlushkou, S. Khirevich, and U. Tallarek, "Pore-size entropy of random hard-sphere packings," *Soft Matter*, vol. 9, p. 3361, 2013.

[55] H. Herrmann, D. Hong, and H. Stanley, "Backbone and elastic backbone of percolation clusters obtained by the new method of burning," *J. Phys. A*, vol. 17, 1984.

[56] M. Newman and R. Ziff, "Efficient monte carlo algorithm and high-precision results for percolation," *Phys. Rev. Lett.*, vol. 85, p. 4104, 2000.

[57] J. Hoshen and R. Kopelman, "Percolation and cluster distribution. i. cluster multiple labeling technique and critical concentration algorithm," *Phys. Rev. B*, vol. 14, p. 3438, 1976.

[58] K. Hawick, A. Leist, and D. Playne, "Parallel graph component labelling with gpus and cuda," *Parallel Computing*, vol. 36, p. 655, 2010.

[59] W. Press, S. Teukoisky, W. Vetterlingand, and B. Flannery, *Numerical recipes*. Cambridge, 3 ed., 2007.